Probabilistic Performance-Based Geometric Tolerancing of Compressor Blades

by

Caroline Marie Lamb

B.S., Massachusetts Institute of Technology (2003)

Submitted to the Department of Aeronautics and Astronautics
in partial fulfillment of the requirements for the degree of

Master of Science in Aeronautics and Astronautics

at the

MASSACHUSETTS INSTITUTE OF TECHNOLOGY

March 2005

Author .....
Department of Aeronautics and Astronautics
March 18, 2005

Certified by .....
David L. Darmofal
Associate Professor of Aeronautics and Astronautics
Thesis Supervisor

Accepted by .....
Jaime Peraire
Professor of Aeronautics and Astronautics
Chair, Committee on Graduate Students

Probabilistic Performance-Based Geometric Tolerancing of Compressor Blades

by

Caroline Marie Lamb

Submitted to the Department of Aeronautics and Astronautics
on March 18, 2005, in partial fulfillment of the
requirements for the degree of
Master of Science in Aeronautics and Astronautics

Abstract

The relationship between tolerances of statically measured geometric parameters and the aerodynamic performance of a sample of manufactured airfoils is investigated in this thesis. The objective is to determine which geometric parameters are the best discriminators of performance, and how these best discriminators are affected by changes in design methodology, manufacturing precision, and desired minimum performance levels. A probabilistic model of geometric variability for a three-dimensional blade is derived. Using this geometric variability model, probabilistic aerodynamic simulations are conducted to analyze the variability in aerodynamic performance. Tolerance optimization is then applied, in which allowable ranges for each geometric parameter are determined so as to maximize the quality of the accepted blades. Optimization is performed at several performance limits to observe how the effectiveness of tolerances and the best geometric discriminators of perfromance change with performance limit. A set of compressor blade data is used consisting of an original geometry, a deterministic re-design, and a probabilistic re-design. Using the geometric variability model, the variability is also artificially increased to investigate the impact of manufacturing precision on tolerance effectiveness. Results shows the best geometric indicators of performance are leading-edge thickness and measures pertaining to the curve quality of an airfoil. While design can affect the performance of tolerances, tolerances are no less effective on probabilistic designs than deterministic designs. Additionally, manufacturing precision affects the best geometric indicators of performance but tolerance effectiveness is not affected.

Thesis Supervisor: David L. Darmofal
Title: Associate Professor of Aeronautics and Astronautics

Acknowledgments

Acknowledgments

This research has been tremendously rewarding and enriching personally, but research is not carried out in a vacuum. I am indebted tot he following people, without which this research wold not have been possible.

- Prof. David Darmofal–for his guidance and good humor throughout what was at times a stressful experience.
- Dr. Victor Garzon–from whose research this topic arose and whose patience never faulted during the many, many questions I asked him.
- Mr. Jeff Lancaster–for the all important data and his expertise in airfoil tolerancing.

I would also like to thank my husband, Andrew, for his encouragement and support. Thanks also to my family for their support and active interest in my research.

This research was supported by fellowships from the MIT Department of Aeronautics and Astronautics and the National Defense Science and Engineering (NDSEG) fellowship program.

Contents

List of Figures

List of Tables

Chapter 1

Introduction

This chapter will introduce the research topic, performance-based geometric tolerancing. Motivations for this line of research (Section 1.1) are presented. In addition, the research objectives are stated (Section 1.2) and a road map for this thesis is presented (Section 1.3).

1.1 Motivation

Decisions made during the design, manufacture, and quality control of a compressor blade affect the final product. For example, assumptions made during design impact performance, manufacturing choices affect the accuracy and precision of the product, and judgments made during quality control ultimately decide what does and does not constitute an acceptable part.

To put the problem in perspective, consider the impact of manufacturing variability on a single compressor blade. Figure 1-1 shows the impact of actual manufacturing variability on the total pressure loss of an airfoil. The effect of variability is a mean loss greater than the nominal loss of the airfoil. In fact, very few of the manufactured airfoils perform at or below the desired loss. When this loss distribution is imposed on each blade row in a six stage compressor (Figure 1-2), the effect is an average reduction in efficiency of 1.2% as compared to the design intent efficiency, with none of the simulated compressors performing on design.

The previous example shows the obvious benefits of controlling variability. The current means used to control variability are to impose tolerances and/or to utilize

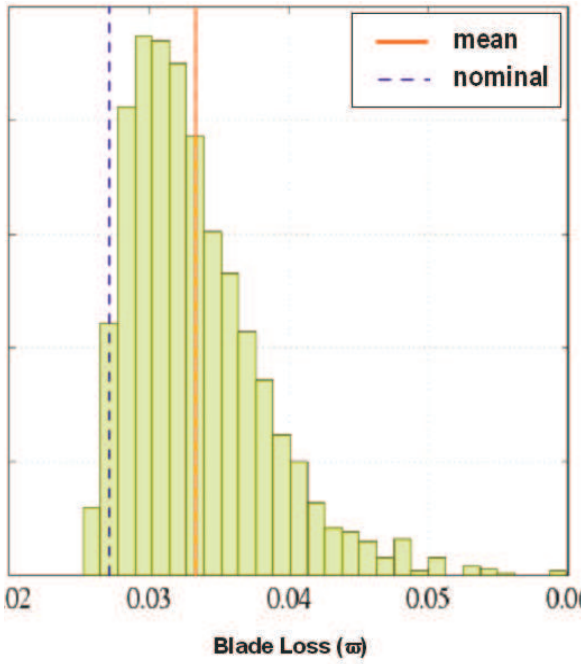

Figure 1-1: Histogram of total pressure loss for manufactured compressor blades [8].

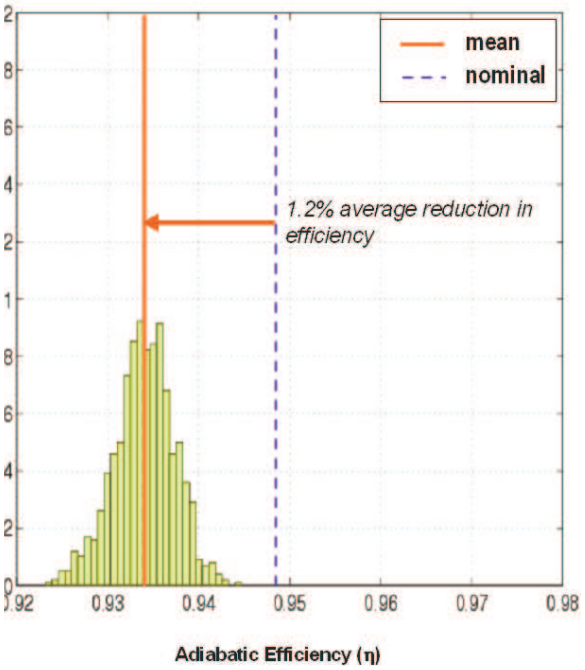

Figure 1-2: Histogram of effect of manufacturing variability on a sample of probabilistic six-stage compressors [8].

more tightly-controlled manufacturing processes. During the course of this thesis, a third and newer method, probabilistic design, will also be discussed.

For now, consider only the use of tolerances to control variability. Tolerances work to reduce *performance* variability by accepting or rejecting blades based on *geometric* variability. However, the relationship between geometric parameters and aerodynamic performance is complex. The result is that geometric parameters are imperfect indicators of aerodynamic performance, as demonstrated in Figure 1-3. Consider a sample of manufactured compressor blade airfoils for which it is desired to keep only the top 90% of the airfoils, rejecting the remaining 10%. Figure 1-3 shows a scatter plot of these blades using two geometric parameters, specifically minimum and maximum leading edge profile. The minimum and maximum leading edge profile are the inward and outward deviations in the manufactured geometries, relative to the nominal geometry. These parameters are discussed more thoroughly in Section 4.2. Those blades marked by a circle are those with performances in the top 90%, and the crosses mark the bottom 10%. It can be seen that minimum leading-edge profile is a poor discriminator of performance while maximum leading-edge performance is a stronger, albeit flawed discriminator of performance. The solid lines bisecting the scatter plot are the tolerancing limits for each parameter. Appropriately no quality control decisions are made on the basis of minimum leading-edge profile while several decision (not all correct) are made on the basis of maximum leading-edge profile.

Recent research has put manufacturing variability into a quantitative framework and also proposed methods to improve airfoil design to more robustly handle geometric variability [10, 22]. However, less attention has been given to the impact of quality control on the resulting airfoil populations. The general premise of performance-based airfoil tolerancing has been explored [11], but not within the constraints of current quality control processes. In addition, the question of how quality control will be affected by airfoils designed with reduced sensitivity to variability has not been addressed.

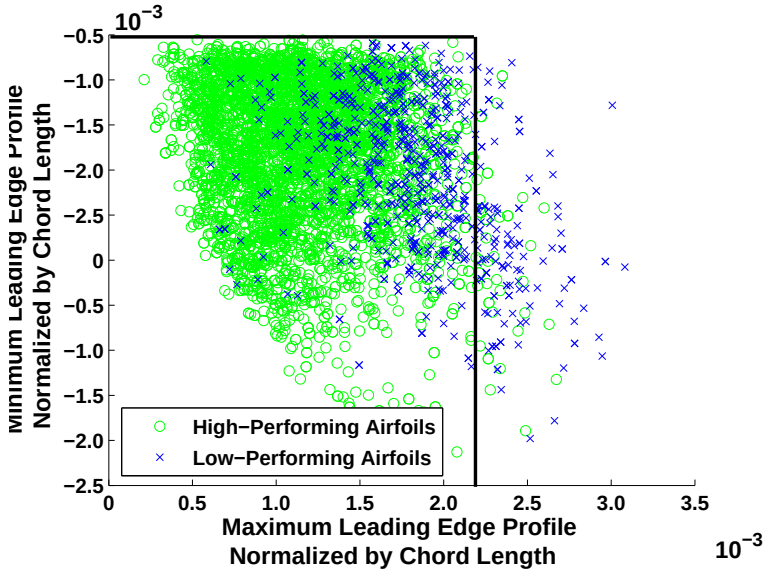

Figure 1-3: Scatter plot of maximum and minimum leading edge profile.

1.2 Research Objectives

This research builds upon previous work. As such, the objectives are inspired by recommendations for future work put forth in Chapter 6 of Garzon's *Probabilistic Aerothermal Design of Compressor Airfoil* [8]. The primary goal is to use the tools and resulting airfoil designs developed by Garzon to both quantitatively and qualitatively evaluate current compressor airfoil quality control practices. Additionally, the impact of probabilistic design and manufacturing precision upon the effectiveness of these quality control practices will be investigated.

To achieve the goals put forth above, the following objectives have been formulated. The first and fifth objectives pertain to steps necessary to achieve the remaining objectives, those pertaining to evaluating tolerance effectiveness.

1. Adapt the manufacturing variability model [8] for use with full three-dimensional (3D) blade geometries.
   (a) Modify the existing two-dimensional (2D) framework to incorporate variability along all three axes.
   (b) Validate assumptions made when using manufacturing variability model to create samples of geometries for Monte Carlo Analysis.

2. Determine the effectiveness of current tolerancing practices.
3. Quantify the impact of probabilistic design on the effectiveness of tolerancing.
4. Quantify the impact of manufacturing precision (magnitude of geometric variability) on tolerancing effectiveness.
5. To achieve the above objectives, develop a means to set optimal ranges on each toleranced parameter given aerodynamic performance data.

1.3 Organization

The previous chapter has motivated performance-based geometric tolerancing as a topic worthy of further investigation. The remaining chapters in this thesis will provide background on the topic and outline the techniques used to explore performance-based tolerancing and the results of that investigation.

Chapter 2 introduces past research, including the work that inspired this research and two views on quality control: current practices and a novel approach put forth in previous research. Figure 1-4 shows the basic outline for Chapters 3-5. Chapter 3 details the modification and validation of the manufacturing variability model used to create probabilistic compressor blade samples. Chapter 4 presents the remaining analysis tools used during the course of research. The results are then discussed in Chapter 5. Concluding remarks and suggestions for future work are put forth in Chapter 6.

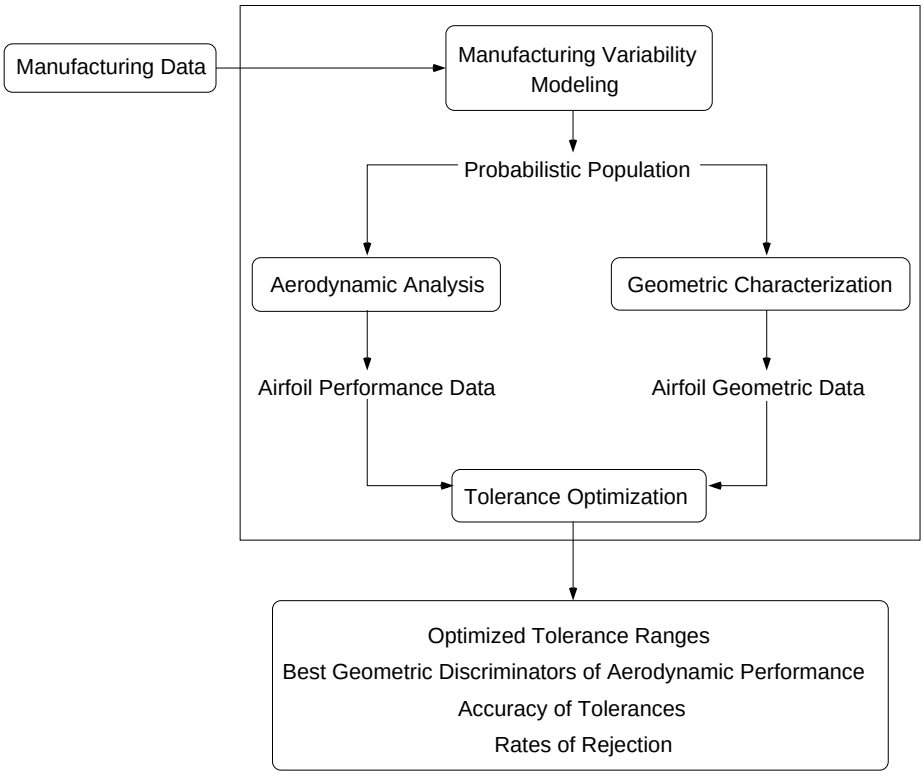

Figure 1-4: Data Analysis Flow Diagram

Chapter 2

Background

The outline of this chapter will follow the three life-cycle stages of interest: design, manufacture, and quality control. Section 2.1 introduces a few commonly used design techniques and a specific probabilistic design technique, the impact of which is investigated in this research. Section 2.2 discusses two manufacturing processes commonly used for compressor blades, establishing the choice of manufacturing process as an important determiner of the magnitude of geometric variability introduced during manufacture. The last section, Section 2.3 summarizes commonly used inspection techniques, introduces the basic ideas used during quality control, and discusses previous research on improving quality control methods for compressor blades using aerodynamic performance.

2.1 Design

A brief review of airfoil design techniques is presented in this section along with an introduction to the airfoil designs used during the course of this research.

Airfoil design methods can be separated into deterministic and probabilistic (also referred to as non-deterministic) approaches. Within each category a variety of methods exist, however, this section will only discuss the overarching principles of each. The airfoil designs used during the course of research represent both deterministic and probabilistic design.

2.1.1 Deterministic Design

Single and mulit-point design optimization are two commonly used deterministic airfoil design methods. As implied by its name, single-point design acts to minimize the "expected cost" of a design at a given, single operating condition[16]. An example of a single-point optimization would be designing a wing airfoil for maximum lift over drag at cruise conditions. Designs produced using single-point optimization by definition perform well at their design point. However, such designs often perform poorly at other operating conditions[16, 5]. For instance, the wing airfoil above may be ill-suited for take-off conditions. In this thesis, comparisons will be made between a nominal compressor blade meanline airfoil geometry and re-designs to improve upon aerodynamic performance. The original meanline airfoil geometry, denoted as ORG, is shown in Figure 2-1. All designs are evaluated at the operating conditions shown in Table 2.1. The deterministic minimum loss airfoil (DML in Figure 2-1) resulted from single-point optimization about the specified operating conditions with the objective of minimizing total pressure loss while maintaining the same turning angle as the ORG airfoil[10].

Assumed Operating Conditions	
Mass Flow Rate	20 kg/s
Wheel Speed	11460 RPM
Tip Speed	301 m/s
Axial Mach	0.43
Inlet Temperature	390 K
Inlet Pressure	200 kPa

Table 2.1: Assumed operating conditions

Multi-point design optimization works in much the same way as single-point optimizations. The primary difference is the designation of multiple operating points about which to optimize. Commonly chosen operating points include combinations such as take-off and cruise, or a set of conditions representing small perturbations about the nominal conditions. Multi-point optimization designs can have a larger

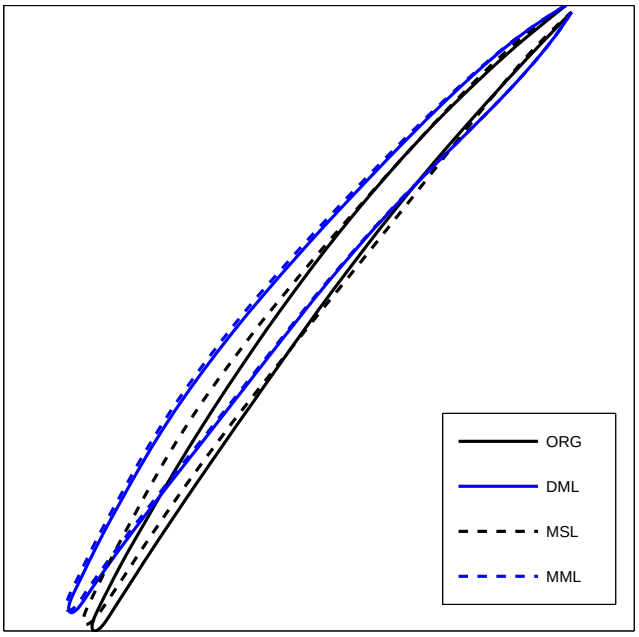

Figure 2-1: Single-point and probabilistic airfoil geometries

range of on-design performance than single-point optimization designs, but the problem remains as to which operating conditions should be chosen as design points and what relative weightings should be used during optimization[16]. Probabilistic design addresses these concerns.

2.1.2 Probabilistic Design

Probabilistic design is a relative newcomer to aerodynamic optimization. Design approaches incorporating variability have been successfully used for years in other fields, the most famous application being the Taguchi method's application in the automotive industry.

The goal of probabilistic design is to achieve designs more robust to uncertainties in manufacturing and operation. Geometric uncertainty is introduced during manufacture or as a results of part wear and repair work[20]. Uncertainty in an airfoil's operating conditions could include perturbation in flow angles, back pressures,

and Mach numbers to name a few sources. These variations, both geometric and in the operating conditions, are often difficult to measure or can only be measured after the airfoil has been manufactured. The difficulty in probabilistic design is to smartly choose or otherwise obtain perturbation distributions to model parameter uncertainty. Given parameter distributions, design of the airfoil geometry then proceeds with some stated design goal. Examples of probabilistic design goals include maximizing the expected value of performance for a range of perturbations or minimizing the performance spread for a range of perturbations[16].

The probabilistic design technique evaluated in this research addresses geometric uncertainty introduced during manufacturing. The method requires a priori knowledge of the manufacturing variability. This knowledge is gained through measurements taken from a sample of actual manufactured compressor blades. The measurements were then used to "desensitize" the nominal design using gradient-based probabilistic optimization. In this method, the optimization structure consists of an optimizer, a variability model, and an aerodynamic analysis code[8]. The variability model is used to apply expected geometric perturbations to the nominal geometry. The aerodynamic performance of each blade is determined using the aerodynamic analysis code and the results are fed to the optimizer which makes small, iterative changes in the nominal geometry until the performance goals are met[10]. This technique was used on the remaining two airfoil geometries in Figure 2-1. The minimum mean loss (MML) airfoil is designed to minimize the expected total pressure loss for a constant average turning angle. The minimum standard deviation loss (MSL) airfoil is optimized for a minimum standard deviation of total pressure loss for a constant average turning angle[8]. The assumptions and techniques used to model manufacturing variability are presented in greater detail in Chapter 3.

2.2 Manufacturing

The choice of manufacturing technique affects the geometric variability introduced. However, the choice of manufacturing method is not solely driven by a desire to reduce

variability. Tradeoffs such as time and cost are also important. The following is an introduction to two commonly used methods for manufacturing compressor blades, point and flank milling, and the tradeoffs associated with each method.

2.2.1 Point Milling

As the name implies, point milling uses the tip, or point, of a tool to remove channels of material to form shapes. Point milling is suitable for nearly any geometry and utilizes standard three or four axis milling machines. In addition, point milling uses standard tooling and can accept standard CAD/CAM commands. These capabilities result in a relatively inexpensive manufacturing process with minimal lead time[21].

However, point milling has its disadvantages. The rounded tool tip leaves small ridges in between passes. These ridges are often in the streamwise direction, and thought to have only a small impact on flow quality. Ridge size is determined by the spacing in between tool passes, and so the only way to minimize the ridges is to reduce the spacing between tool passes. Reduced spacing results in greater tool wear, longer milling times, and therefore increased costs. Perhaps the greatest disadvantage of point milling is that it is rarely a stand-alone process but is used in combination with other finishing processes such as peening and hand grinding of the leading and/or trailing-edges. These additional processes increase the opportunity for variability in the finished product.

2.2.2 Flank Milling

Flank milling is a less commonly used process utilizing the side, or flank, of the tool to remove material. By using the side of the tool, two disadvantages associated with point milling are improved: tool life and surface quality. The increased surface area used to remove material extends tool life, and also improves surface quality by eliminated the ridges associated with point milling. Surface quality is also improved by the ability of flank milling to stand alone as a single process capable of milling both the main geometry and the leading and trailing-edge details[21]. One estimate

of the benefit of flank milling places the overall geometric variability of a flank milled compressor blade as one-sixth that of a comparable point milled compressor blade[8].

The disadvantages of flank milling are in its limited applicability and increased costs. Because the sides of the tool are used to remove material, custom tooling is required for each geometry. In addition, not all geometries are suitable for flank milling. This requires that both the manufacturing method and tooling be considered during design. Flank milling also uses five-axis milling machines, which are more expensive and less common. Special software is necessary to translate designs into flank milling tool trajectories.

2.3 Quality Control

The goal of inspection and quality control is to measure parts and to pass or fail them on the basis of those measurements. Pass and fail decisions are made by considering the impact of geometric perturbations on the final assembly, where the allowable perturbations are determined by backing out limits for each measurement based on the limits of allowable performance. In the case of static assemblies these limits, or tolerances, assure that individually manufactured pieces will interface properly [13]. For example, the peg in Figure 2-2 will fit into the hole for all combinations of allowable peg and hole diameters.

However, in a dynamic system such as an aircraft engine compressor, judgments about an airfoil's *dynamic performance* are made using *static geometric measurements*. Tolerances on these geometric measurements are set with consideration for the capabilities of the manufacturing process being used as well as the impact of variation in each measurement on compressor performance. In the case of a compressor blades, both structural and aerodynamic performance must be considered.

The following sections introduce how static geometric measurements are taken and translated into pass or fail decisions for compressor blades.

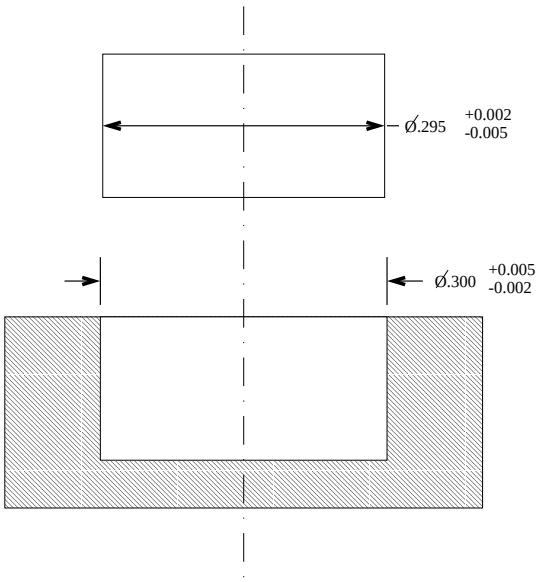

Figure 2-2: Diagram of a peg and slot interface with tolerances

2.3.1 Inspection

Each chord-wise cross section of a compressor blade is an airfoil that can be described in terms of familiar and meaningful geometric parameters such as chord length and incidence angle. Inspection methods therefore treat compressor blades as a set of measured airfoils, measured a preset spanwise locations of interest. The measurements from these airfoil cross-sections are used to judge part acceptability. The following inspection techniques describe how these data are obtained in reference to a single blade cross section or airfoil.

Computer, or Coordinate Measuring Machines (CMM's) collect data via a small computerized probe that scans the blade surface at some set of predetermined locations[13]. From this, a set of coordinate inspection points describing the airfoil is produced.

CMM data are subject to error caused by the effects of temperature, humidity, and movements of the part being inspected. Errors associated with temperature and humidity are controlled by conducting CMM inspections in controlled environments[13]. Errors associated with part movement are not significant on the scale of most geometric parameters of interest. However, there is concern that small movements induced in the airfoil by the act of inspection are significant enough to introduce error into the

thinner, more flexible leading and trailing-edge regions with magnitudes comparable to the leading and trailing-edge radii.

New inspection methods under developments utilize lasers and holographic techniques. These new methods do not require blade geometries to be broken down into airfoil cross sections. Rather, the complete three-dimensional geometry is scanned and used for quality control purposes[13].

2.3.2 Quality Control

After inspection data are collected, those data are converted into useful forms. In the case of CMM data, this involves converting sets of coordinate data into chord lengths and leading-edge angles and thicknesses, to name a few parameters. These descriptive metrics are then used for quality control decisions. As stated earlier, the goal of quality control is to assure some minimum *dynamic* part performance. To this end, allowable ranges for each geometric parameter are set.

A typical quality control process for compressor blades begins by comparing the measured geometric parameters to their allowable ranges. If any single metric falls outside the allowable ranges, the airfoil is conditionally failed and sent for a more detailed inspection. During the more detailed inspection, the airfoil is re-measured and aerodynamic and/or structural simulations can be executed to more accurately estimate the airfoil's performance. If simulations indicate acceptable dynamic performance, the airfoil passes inspection and tolerancing ranges might be changed to pass similar airfoils in the future. Conversely, if simulations indicate an unacceptable dynamic performance, the airfoil is failed and either sent for re-work or scrapped.

Limits on the allowable range for each geometric parameter are set with consideration for aerodynamics, structures, and past experience with similar geometries and manufacturing processes. However, there is no guarantee that the limits used are optimal, and there is no consideration of the coupling effect of an airfoil being near the limit of several parameters as opposed to just one parameter.

Commonly-used measured parameters include chord length, leading-edge and trailing-edge thicknesses, leading-edge angles, chord angles, and various measures of surface

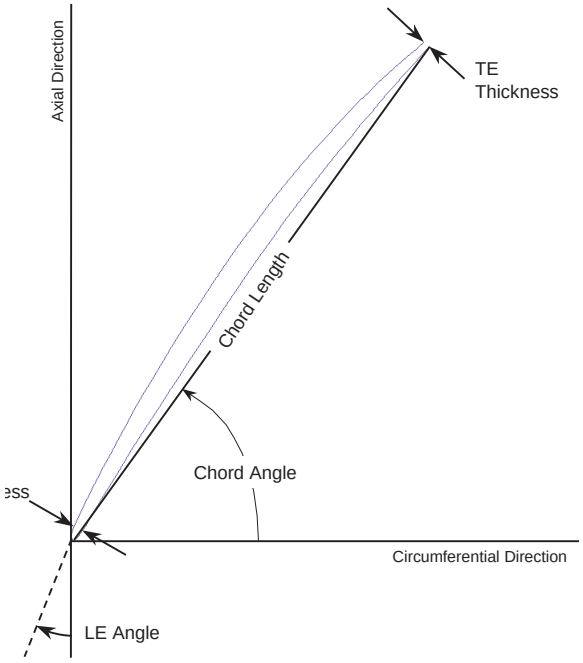

Figure 2-3: Airfoil geometry labeled with common geometric parameters

quality. Figure 2-3 shows an airfoil labeled with five of the commonly used geometric parameters. A more in-depth discussion of these parameters and an introduction to additional surface quality parameters is presented in Section 4.2.

An attempt to improve the decision-making process was proposed by Häcker[11] who used a comparison method based on Malahanobis distance arrays to classify airfoils. The methods utilized a large training population for which the aerodynamic performance was known. Inspected airfoils were then compared to those in the training population using the Malahanobis distance as a measure of similarity. The Malahanobis distance is the magnitude of an array of parameter differences where each difference is scaled by the inverse of that parameter's variance. Under this scheme, the inspected airfoil receives the same classification, pass or fail, as the airfoil in the training population to which it has the smallest Melahanobis distance[11]. The strength of Häcker's system is that it implicitly accounts for the coupling between measured parameters. Häcker's system captures performance impacts caused by a confluence of perturbations not captured by looking at each parameter independently. Lacking

from Häcker's method, however, are the familiar geometric parameters that facilitate understanding of how the geometry is perturbed.

The tolerance optimization method proposed in this research attempts to improve currently-used quality control methods by improving understanding of which parameters best indicate performance, if the best indicators change with design method and/or level of variability, and by using probabilistic data to set the allowable parameter limits.

Chapter 3

Geometric Variability Model

Referring to Figure 1-4, this chapter covers the first step in data analysis: the geometric variability model used to create probabilistic samples of compressor blades for aerodynamic analysis.

Section 3.1 describes in detail Principal Components Analysis (PCA), the technique implemented by Garzon[8] to quantitatively describe manufacturing variability observed in compressor blades. Specifically, a brief treatment of the theory behind PCA is presented followed by a discussion of the differences in implementation relative to Garzon's work and the inherent statistical uncertainty of PCA.

Section 3.2 then shows how PCA is used to create probabilistic compressor blade samples for Monte Carlo Analysis inputs. An in-depth discussion of the assumptions made during the formation of probabilistic blade samples is also presented in Section 3.2.

3.1 Principal Components Analysis

The goal of the manufacturing variability model is to facilitate the generation of large probabilistically accurate samples of compressor blades based on a smaller initial sample taken from measurements of actual manufactured artifacts. These large probabilistic samples by definition must have the same patterns of geometry variability and performance as the initial sample. To this end, Principal Component Analysis (PCA) is used to create a high-fidelity model of the geometric variability introduced

during the manufacture of compressor blades.

The compressor blade manufacturing data come from coordinate-measuring machine (CMM) measurements of 105 nominal-identical flank milled blades. The CMM definition of each blade is defined by 13 radial cross sections, or airfoils, each consisting of 112 points. The measurements are of the static blade geometry, and any operational changes in blade due to thermal expansion, elongation, or untwist due to centrifugal loads experienced during operation are not included.

3.1.1 Principal Components Analysis

Long used in fields such as weather forecasting and image processing, PCA techniques were developed as early as the 1870's[19]. More recently, PCA has found favor in reduced-order modeling applications. In his thesis, Garzon outlines the use of PCA to create a model of compressor blade geometric variability based on a set of measured blade geometries[8]. The basic premise is to break the measured geometries into a nominal geometry, an average perturbation, and a set of orthogonal, or independent, perturbation geometries. The following description of PCA is adapted from Garzon's work[8].

PCA, as applied here, refers to the decomposition of a set of geometries into a nominal geometry, x^0, an average observed perturbation, $\bar{x}$, and a set of n orthogonal modal geometries, x_i. Each geometry is composed of p m-dimensional points and represented by a vector of length mp. As shown in Equation 3.1,

$$\hat{x_j} = x^o + \bar{x} + \sum_{i=1}^{n} a_{ij} x_i, \tag{3.1}$$

each measured geometry, $\hat{x_j}$, can be expressed as the sum of the nominal geometry, the average perturbation and the weighted sum of each of the n modal geometries, $a_{ij}x_i$. Of the parameters in Equation 3.1, x^o is known, and $\bar{x}$ is calculated directly from the blade sample. The modal geometries and amplitudes, x_i and a_{ij}, are the outputs of PCA.

To calculate the modal geometries and amplitudes, first consider a matrix, X, in

which each row describes the perturbation of a single measured blade, $\hat{x_j} - x^o - \bar{x}$. Given there are N measured blades, each described by p m-dimensional points, the dimensions of X are N by mp. The scatter matrix, S, of X is defined as,

$$S = X^T X. \tag{3.2}$$

The eigenvectors and eigenvalues of S correspond to the modal geometries and the variances (σ_i^2) of the corresponding modal amplitudes (a_i). Because the modal geometries are described by eigenvectors of a symmetric matrix, the modal geometries are by definition orthogonal. The rank of S, and therefore number of modal geometries, is at most $n = \min\{N, mp\}$. For the case under consideration $n = (N-1)$, indicating any blade in the initial sample can be fully described using the set of $(N-1)$ modal geometries. The mean perturbation, which was removed from X, can be thought of as the N^{th} modal geometry with a corresponding amplitude of 1. The scatter matrix is also a scalar multiple of the covariance matrix, C, of X,

$$C = (n-1)^{-1} S. \tag{3.3}$$

As such, the modal geometries are uncorrelated by definition. This does not imply the modal geometries occur independently of each other, a point discussed in Section 3.2.

An analogous way to explain PCA is by comparison to the *Singular Value Decomposition* (SVD) of matrix X,

$$X = U \Sigma V^T, \tag{3.4}$$

where the columns of V are equivalent to the eigenvectors of S, the Σ matrix is a diagonal matrix whose entries are equal to the square root of the eigenvalues of S, and U contains the contribution of each modal geometry in the compositions of each measured blade geometry. The product $a = U\Sigma$ is a matrix containing the modal amplitudes (a_{ij}) used to determine the amplitude of the i^{th} modal geometry, x_i, required to reconstruct the j^{th} blade from the initial sample.

For a more detailed introduction to PCA, please refer to Chapter 2 and Appendix A of reference [8].

3.1.2 Impact of Model Dimension, m

In his research, Garzon worked primarily with 2-dimensional PCA, that is $m = 2$.[1] All of the PCA used in thesis is based upon a 3-dimensional model of geometric manufacturing variability.

As mentioned above, PCA is often used in reduced-order modeling. Therefore, it is of interest to note the number of modes required to capture most of the observed geometric variability. With a 2-dimensional PCA model of geometric variability, that is considering the variability along each airfoil section independently, 99% of the observed variability is contained in the first six modal geometries, as shown in Figure 3-1(a). When the blade geometries were analyzed as a 3-dimensional whole, the required number of modal geometries to capture 99% variability jumps to 28 (Figure 3-1(b)). The impact of this "spreading" would likely result in increased analysis time in reduced-order modeling applications.

Figure 3-2 shows the relative decay rate of the eigenvalues (mode strengths) for both the 2-dimensional and 3-dimensional models. Despite the increased number of modes required to satisfactorily describe variability, the model eigenvalues still asymptote to a decay rate of one order of magnitude per 20 modes. This is important because it reinforces that the variability content of the remaining modes omitted in reduced-order modeling applications approaches null at the same rate in the 2-dimensional and 3-dimensional models..

These points are mentioned as points of interest. This research is not based on reduced-order modeling and all the modes are used in the subsequent probabilistic simulation and therefore there is no impact observed in this research due to the increased spread.

[1] Garzon presents briefly touches upon 3-dimensional PCA in Appendix A[8].

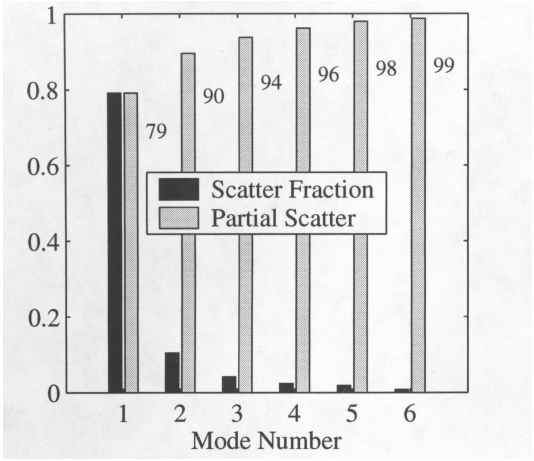

(a) Scatter fraction, partial fraction 2-D

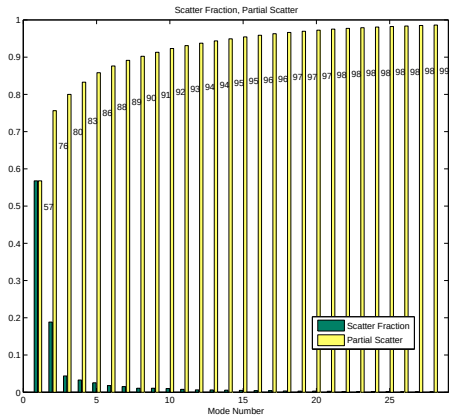

(b) Scatter fraction, partial fraction 3-D

Figure 3-1: Effect of dimension of geometry model

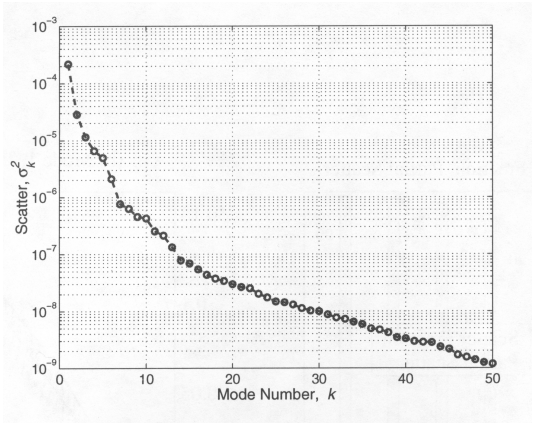

(a) 2-dimensional model eigenvalues

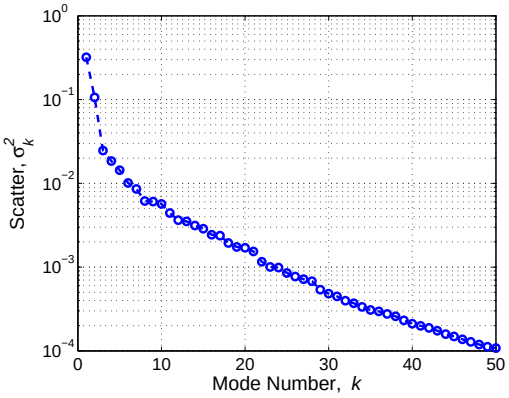

(b) 3-dimensional model eigenvalues

Figure 3-2: Comparison of decay of eigenvalues of S for 2- and 3-dimensional models

3.1.3 Statistical Uncertainty of PCA

Due to the limited size of the initial blade sample, there is some amount of statistical uncertainty present in any further analysis based on outputs of the manufacturing variability model. As the primary outputs of this research will be in terms of probabilities, the statistical uncertainty is also presented in terms of probabilities.

Consider a very large collection of blades for which it is desired to know what percentage, P, has some characteristic, Y. One way to determine the answer is to survey the entire blade population. However, limited data and time and resource constraints might make this infeasible. One might then randomly select of group of N blades as a representative sample of the entire population. There are any number of possible combinations of N blades, each with a slightly different rate of occurrence of Y, $\hat{P}$. These samples are normally distributed with an average value of $E\{\hat{P}\} = P$, and a standard deviation, $\sigma_{\hat{P}}$, that is dependent on both P and the sample size, N[18].

$$\sigma_{\hat{P}} = \sqrt{\frac{P(1-P)}{N}} \tag{3.5}$$

Equation 3.5 shows the standard deviation of $\hat{P}$ is directly related to the product of P and $1-P$ and inversely related to the sample size, N. The 95% confidence interval for calculated probability is then $\hat{P} \pm 2\sigma_{\hat{P}}$[18].

There are two sources of uncertainty in the manufacturing variability model. The first is related to the sample size of the original measured compressor blades. In this case, the model is based on an original sample size $N = 105$. Because manufacturing data is limited, increasing N is not an option. The solid line in Figure 3-3 shows the resulting 95% confidence range, $2\sigma_{\hat{P}}$, resulting from the limited size of the measured manufactured compressor blade sample. The small number of original blades, $N = 105$, results in a confidence range of 2% for $P = 1\%$. The break-even point is at $P = 4\%$. For probabilities greater than 4%, the associated uncertainty is smaller than the probability of interest.

The second source of uncertainty comes from the sample size generated for Monte Carlo analysis using the manufacturing variability model. Because these samples are

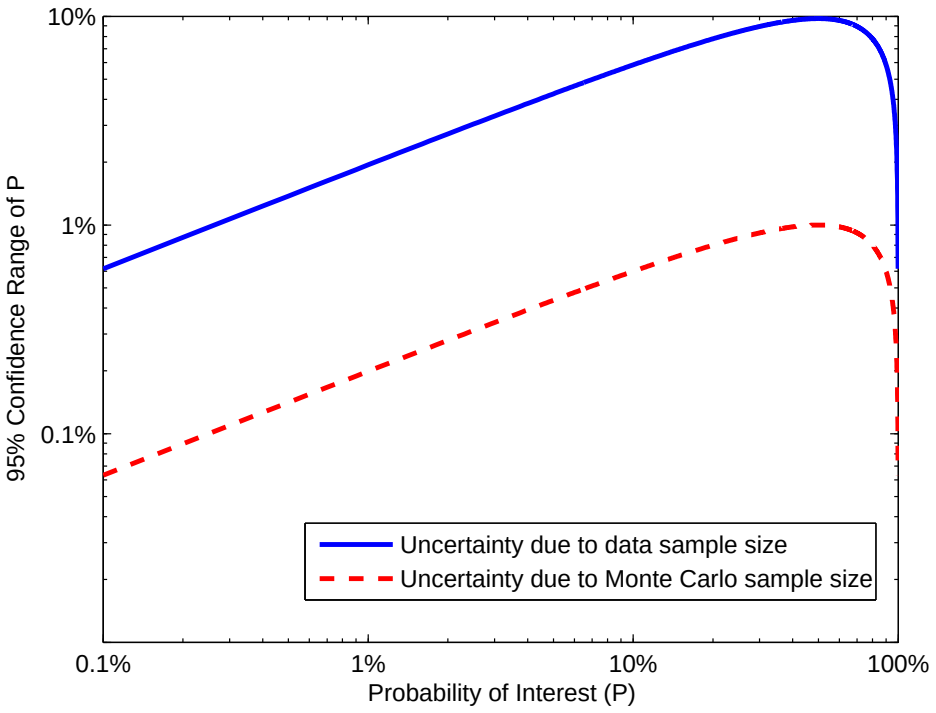

Figure 3-3: Modeling uncertainty for initial sample size $N = 105$, and Monte Carlo sample size $N = 10000$

limited in size, there is some uncertainty as to how well they represent the modeled sample, where as a sample of infinite size would have no uncertainty. The uncertainty contribution from the Monte Carlo sample size can be directly controlled by choosing the probabilistic blade sample size, N in Equation 3.5. It was decided that the uncertainty contributed by the Monte Carlo sample size should be small in comparison to that due to the original sample size. To accomplish this, the uncertainty contribution due to Monte Carlo sample size was kept one order of magnitude smaller than that due to original sample size. As can be seen from Equation 3.5, this requires the Monte Carlo sample size to be 100 times larger than the data sample size. Thus, the Monte Carlo simulations are for 10,000 blades. The 95% confidence range based on the probabilistic sample size is plotted as a dashed-line in Figure 3-3. For $P = 1\%$, the corresponding uncertainty is therefore 0.2%.

3.2 PCA Based Variability Model

The goal of this section is to explain the steps taken and assumptions made to create a probabilistic model representing the original sample of measured blades using the PCA model of manufacturing variability outlined in Section 3.1.

3.2.1 Generating Probabilistic Samples

PCA can be used to created probabilistic blades, $\tilde{x}$, by combining the original parts, shown in Equation 3.1, but replacing the original modal amplitude, a_{ij}, with randomly generated modal amplitudes, $\tilde{a_i}$, as shown in Equation 3.6,

$$\tilde{x} = x^o + \bar{x} + \sum_{i=1}^{n} \tilde{a_i} x_i. \tag{3.6}$$

The second part of this chapter discusses how the random amplitudes, $\tilde{a_i}$ are modeled such that the probabilistic blade geometries, $\tilde{x}$, have the same characteristics as the original measured blade, $\hat{x_j}$.

3.2.2 Modeling Assumptions

A second set of measured blade data is introduced for the purposes of validating the geometric model. The compressor blade data introduced earlier comes from a set of flank-milled compressor blades. The second set of manufacturing data come from a set of point-milled fan blades with hand-finished leading and trailing edges. The fan blades will be used to demonstrate the impact of geometric modeling assumptions because the fan blades are "noisier" than the compressor blades. The fan blades are considered "noisier" on the basis of two measurements of manufacturing variability. The first measurement looks at the RMS,

$$x_{i_{RMS}} = \sqrt{\frac{1}{p}\Sigma_{k=1}^{p}|\sigma_i x_{ik}|^2}, \tag{3.7}$$

of each modal geometry, x_i, normalized for purposes of comparison, by the magnitude of the mean perturbation,

$$\bar{d} = \sqrt{\frac{1}{p}\Sigma_{k=1}^{p}|\bar{x_k}|^2}. \tag{3.8}$$

Figure 3-4(a) shows the mean perturbation relative RMS of each mode for both sets of blade data. The fan blades (represented by solid line) have greater variability content in each mode relative to the compressor blade (dashed line). In addition, only two compressor blade modes have an RMS greater than the mean compressor perturbation. There are eight fan blade modes with an RMS greater than that of the mean fan perturbation. Because the compressor blade mean perturbation is large compared to all but two of the modal perturbations, the compressor blade perturbation is mean-dominated. Deviations from nominal measurements and performance are dominated by the mean perturbation. By contrast, the fan blade mean perturbation is small in comparison to several modal perturbations. As such, the fan blade perturbation is mode-dominated. Deviations from nominal measurements are dominated by the first few modal perturbations. Figure 3-4(b) shows σ_i non-dimensionalized by the corresponding airfoil chord length. The comparison shows the fan perturbations are larger relative to the blade geometry than the compressor blade perturbations.

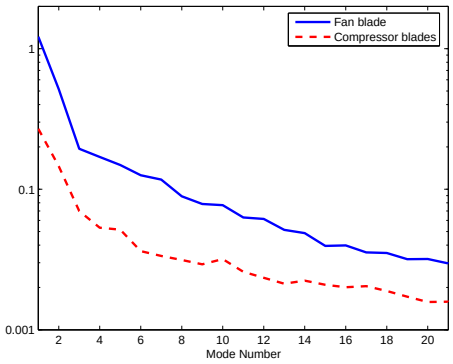

(a) Modal RMS normalized by magnitude of mean perturbation, $\bar{d}$

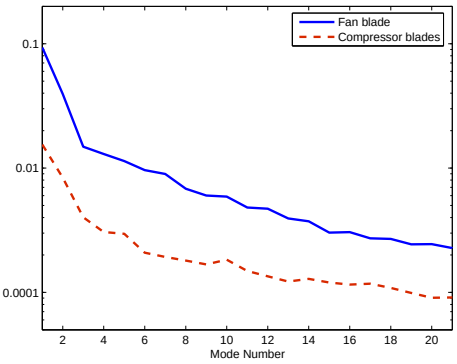

(b) Modal RMS normalized by chord length

Figure 3-4: Comparison of compressor and fan blade variability

The following two sets of graphics show the mean, first, and second mode perturbations for the fan and compressor blades. Each individual graphic maps the perturbation magnitude at each point onto and "unwrapped" blade surface.

Figure 3-5(a) shows the mean compressor blade perturbation. The largest perturbations are near the leading-edge tip and have an amplitude of 0.01. The magnitude of the average point-perturbation is approximately 0.006. The compressor blade first mode perturbation, shown in Figure 3-5(b), is larger than the mean perturbation, with a larger portion of the blade surface having a perturbation amplitude greater than 0.02. Figure 3-5(c) shows the compressor blade second mode perturbation. While there are isolated point-perturbations greater than 0.02, most of the blade surface has a perturbation of less than 0.008, with an average just below that. Subsequent modes have average amplitudes well below that of the mean perturbation, with the average point-perturbation quickly approaching zero.

Figure 3-6(a) shows the amplitude of the mean perturbation at each point on the fan blade surface. A small area near the trailing-edge tip has an amplitude greater than 0.04. Most of the blade surface has a point-perturbation below 0.02. The fan blade first mode perturbation is shown in Figure 3-6(b). A large fraction of the blade surface has a first mode perturbation amplitude greater than 0.1, with an average

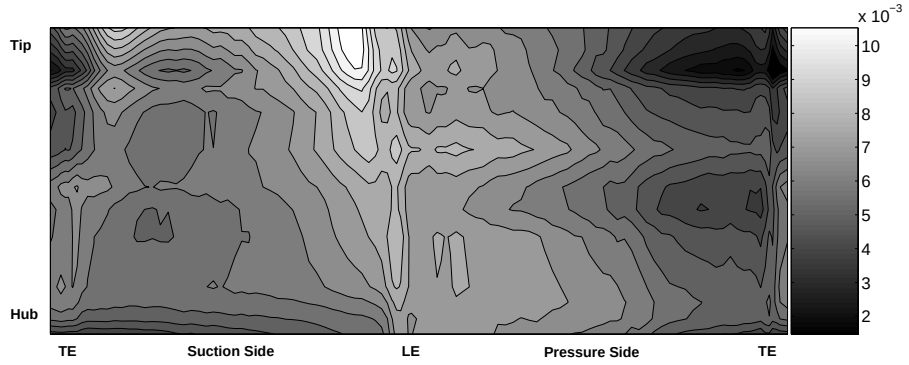

(a) Mean perturbation, $\bar{x}$

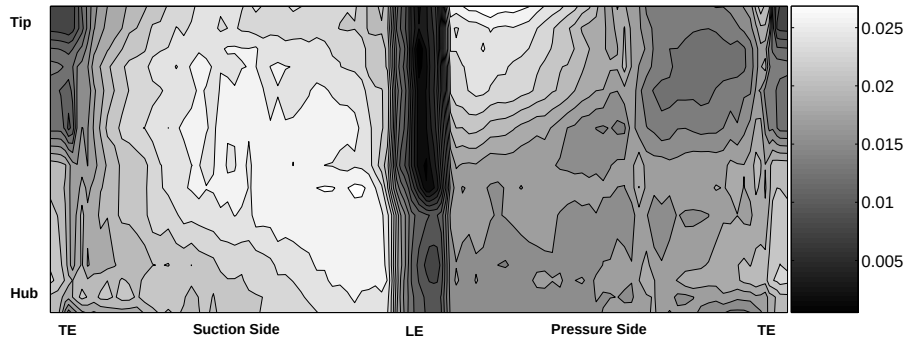

(b) First mode perturbation, $\sigma_1 x_1$

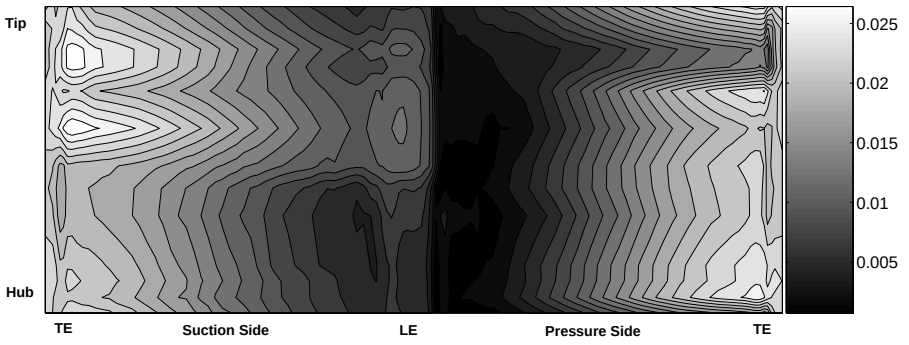

(c) Second mode perturbation, $\sigma_2 x_2$

Figure 3-5: Relative mean and modal perturbations of compressor blades

point-perturbation of about 0.085. The fan blade second mode perturbation, shown in Figure 3-6(c), shows isolated areas near the mid-span leading-edge with perturbation amplitudes near 0.12, with an average perturbation amplitude of approximately 0.6. Until the eight mode, the average modal perturbation exceeds the average mean perturbation of 0.02.

As stated earlier, previous work has generated modal amplitudes by assuming each mode occurs independently and that its amplitudes are normally distributed ($N\{0, \sigma_i\}$), where σ_i is taken from the square roots of the eigenvalues of S (Equation 3.2. However, upon inspection of the fan blade amplitudes it was discovered that the first mode, a_1, is clearly not normally distribution. Figure 3-7 shows the actual distribution of the first mode geometry of the fan blade. The distribution has a distinct bimodal distribution.

Given the bimodal first mode distribution, another approach is to generate the modal amplitudes independently using empirical cumulative distribution functions (CDF) based on the actual original modal distributions, a_i. The use of independent, empirical CDF's captures the bimodal nature of the first mode. However, analysis of the resulting geometries showed the modeled geometries did not have the same distribution of leading edge radius as the original sample.[2] Figure 3-8 shows the 70% span leading edge radius distribution of the original fan blades. Figure 3-9 shows the same distribution based on a set of blades generated using independent, empirical CDF's. The blades exhibit greater leading edge variability than the original manufactured blade sample, suggesting some additional assumption is needed to properly model the original sample.

Upon further investigation, it was found that the first and second modes, while uncorrelated, do not occur independently of each other. Figure 3-10 is a scatter plot showing the first and second mode amplitudes of fan blades in the original measured sample. When the two clusters are inspected independently, their correlation coef-

[2]The same distribution patterns are observed in minimum leading edge-profile measurements, but preliminary aerodynamic analysis showed a stronger correlation between performance and LE radius that minimum LE profile. Therefore, while leading-edge radius is not considered a trusted parameter, it was used during model validation.

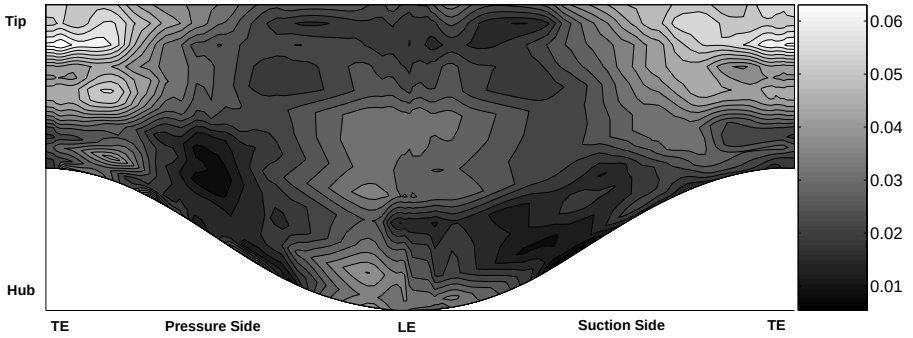

(a) Mean perturbation, $\bar{x}$

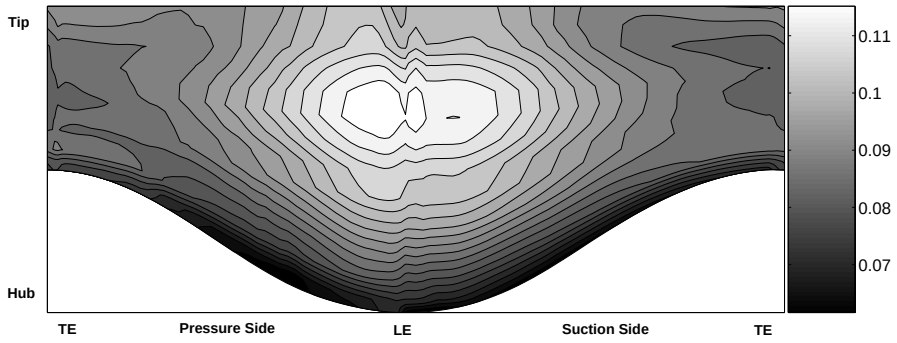

(b) First mode perturbation, $\sigma_1 x_1$

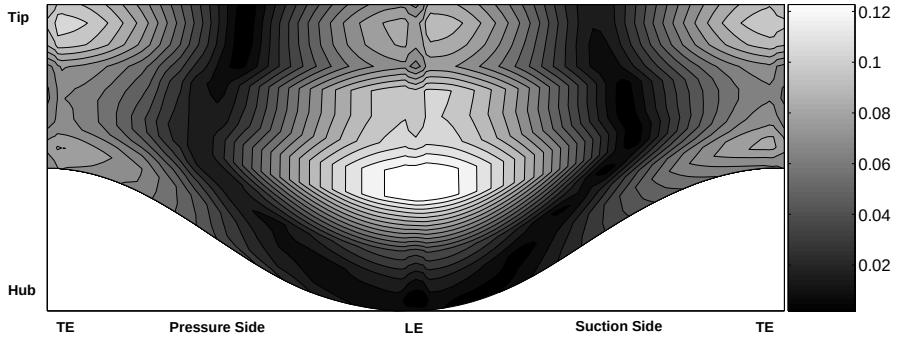

(c) Second mode perturbation, $\sigma_2 x_2$

Figure 3-6: Relative mean and modal perturbations of fan blades

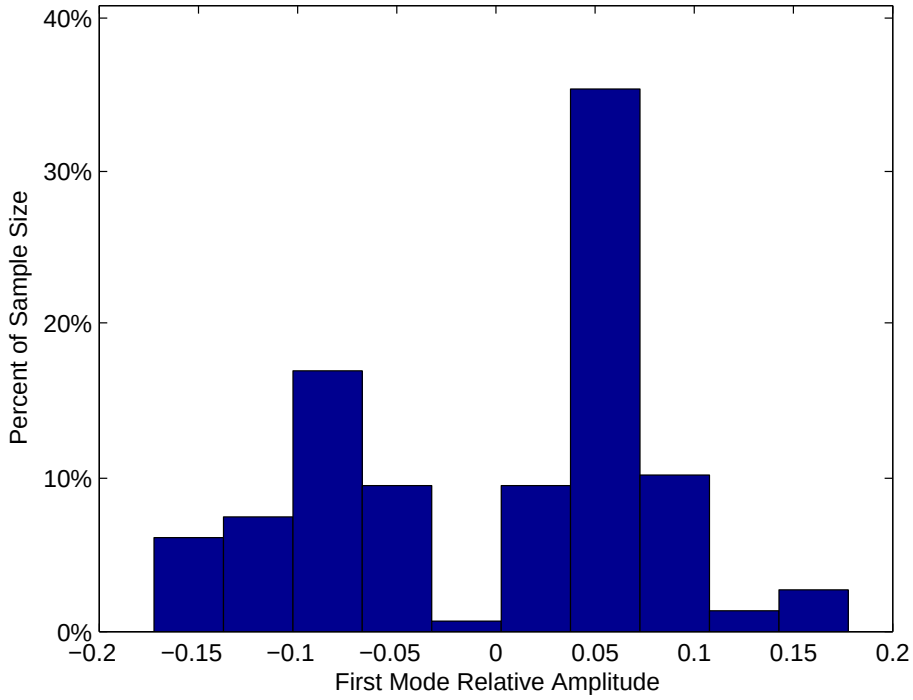

Figure 3-7: Fan blade mode 1 amplitude distribution

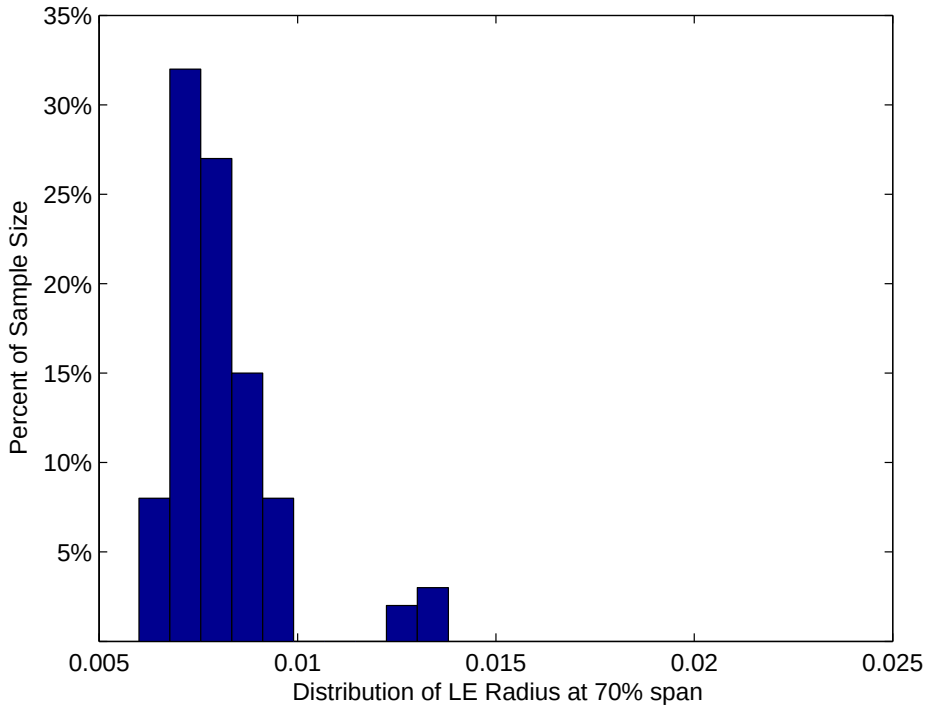

Figure 3-8: Distribution of leading edge radius of original 105 manufactured blades

ficients have magnitude 0.3 and 0.6. This brings about an additional distribution assumption, that the modal distributions are not necessarily independent. However, modeling inter-modal dependencies requires a method by which to generate distributions for dependent data. The method implemented in this data is a non-parametric density estimation technique known as Parzen Windows[2].

The premise of Parzen Windows is to place a d-dimensional normal distribution at each of the N observed vectors of amplitudes (a_j), where d is the number of dependent modes to be modeled, and therefore the length of the vector a_j. The standard deviation, h, is treated as a "smoothing" parameter and is set experimentally such that closely neighboring points blend together to create a smooth distribution but not so large as to loose distinction between distantly neighboring data points. By trial and error, a smoothing constant $h = 0.01$ was chosen. Specifically, the

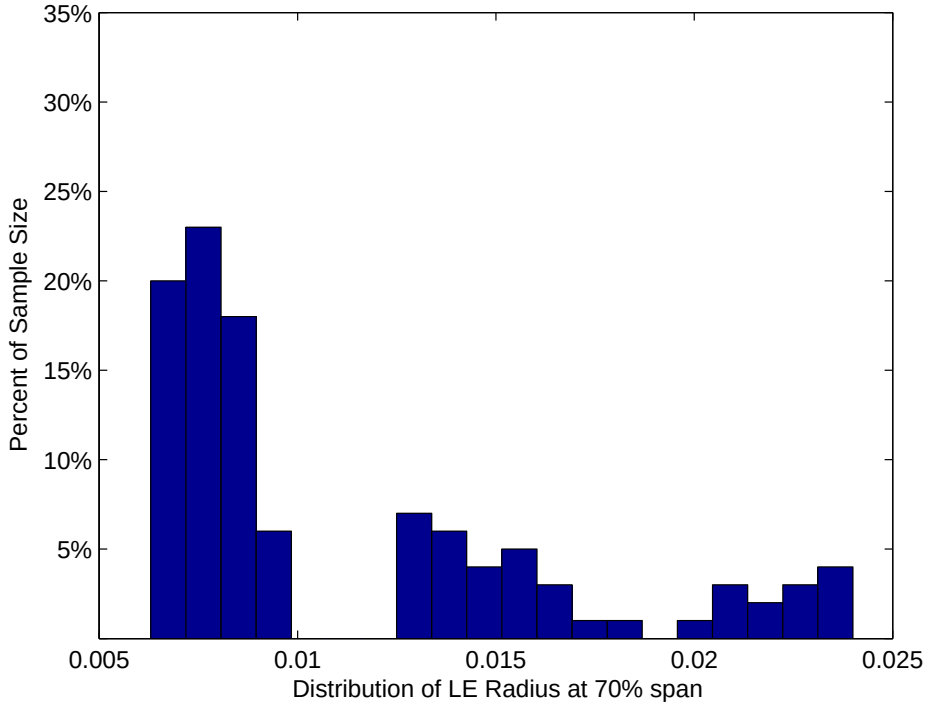

Figure 3-9: Distribution of leading edge radius generated using independent empirical CDF's

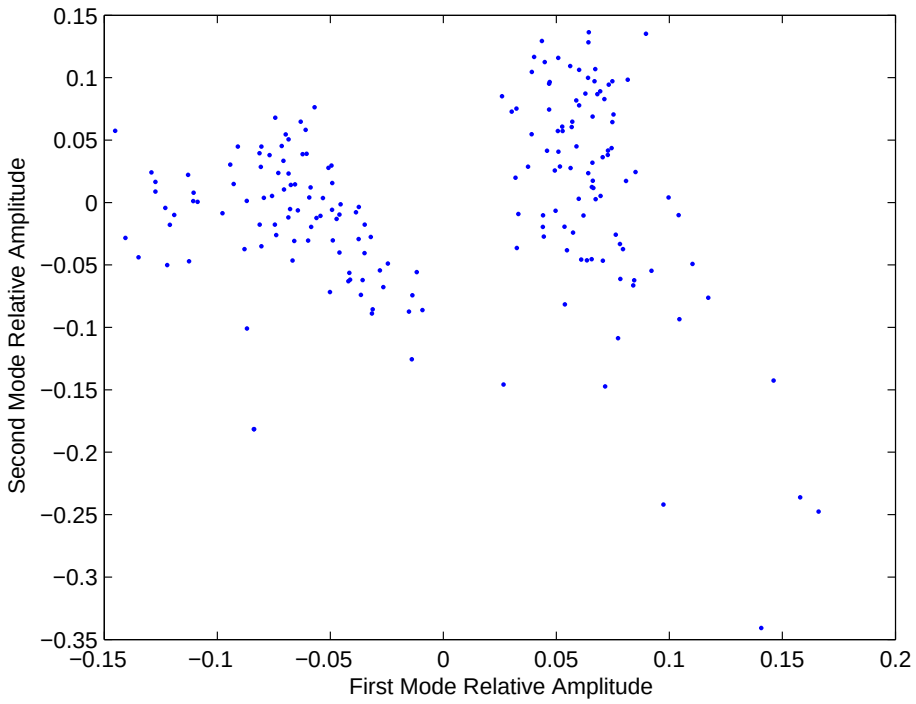

Figure 3-10: Fan blade mode 1 and 2 amplitude distributions

probability density is given by,

$$\tilde{p}(\tilde{a}) = \frac{1}{N}\sum_{j=1}^{N} \frac{1}{(2\pi h^2)^{\frac{d}{2}}} \exp\{-\frac{\|\tilde{a} - a_j\|^2}{2h^2}\}. \tag{3.9}$$

The probability density function resulting for modes one and two resulting from Equation 3.9 is shown in Figure 3-11. Dependencies were observed between the first and second modes as well as between the first and third modes. Inspection of the first ten modes revealed no additional inter-modal dependencies. The remaining modal amplitudes were generated using independent CDF's of the original modal amplitudes a_i.

The leading edge radius distribution resulting from modeling the inter-modal dependencies is shown in Figure 3-12. Compared to the original leading edge radius distribution, shown in Figure 3-8, the generated distribution shows a similar spread in values.

The final modeling assumption is that the observed perturbations can be applied to

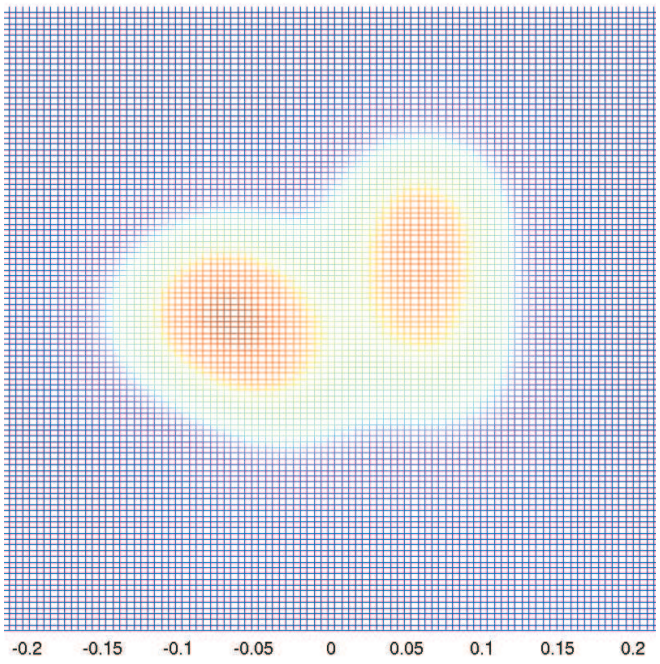

Figure 3-11: PDF for mode 1 and 2 fan blade amplitudes

the redesigned airfoils. The basis for this assumption is that the changes in geometry between the original and redesign airfoils are small and therefore one would expect the manufacturing variability to be similar. Unfortunately, there is no data to evaluate this assumption. As such, it will be assumed that any error introduced by this assumption is negligible.

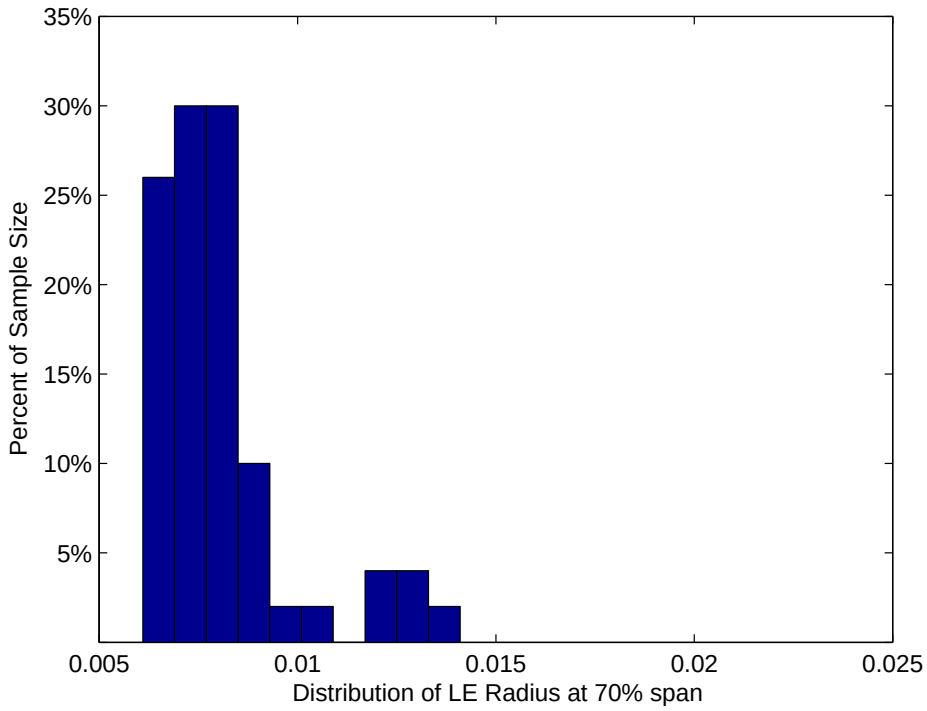

Figure 3-12: Distribution of leading edge radius generated modeling inter-modal dependencies

Chapter 4

Analysis

This chapter covers the remaining analysis steps shown in Figure 1-4: aerodynamic analysis, geometric parameterization, and tolerance optimization.

Aerodynamic analysis produces the performance metric necessary for *performance*-based optimization of tolerances. Section 4.1 consists of a description of the aerodynamic model used to analyze blade performance as well as a discussion of the performance metric chosen for tolerance optimization. Section 4.2 introduces the 14 geometric parameters used in tolerancing.

Finally, Section 4.3 describes how an optimal set of tolerance limits are determined from the aerodynamic performance and geometric parameters of a sample of blades. The importance of this section is two-fold. First, a method for determining optimal tolerances is introduced. Second, the use of optimal tolerances allows for the comparison of tolerance effectiveness across changing designs, performance limits, and manufacturing precision.

4.1 Aerodynamic Analysis

As mentioned in Section 2.1, the focus of this research is the airfoil defined by the meanline streamline of a compressor blade and a set of redesigns of that meanline airfoil.

Due to the probabilistic nature of this research, large numbers of compressor airfoils must be analyzed. MISES, Multiple blade Interacting Streamtube Euler Solver,

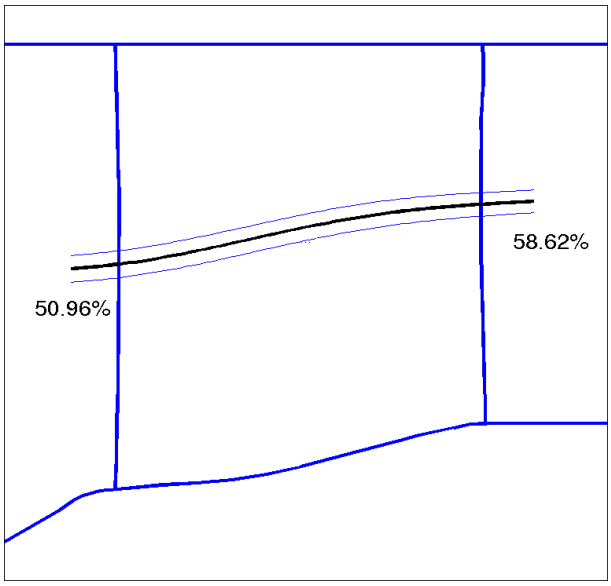

Figure 4-1: Plot of airfoil geometry in axial-radial coordinates with relative position of meanline streamline indicated

was chosen for the aerodynamic analysis module[6] because of its quick solution time[1]. In addition, the framework necessary to analyze the meanline streamline of the blade under investigation was already in place as a result of Garzon's[10] research utilizing the same blade geometries. MISES's speed and strength come from a strongly coupled inviscid-viscous algorithm. Inviscid flow parameters are calculated using steady state 3-dimensional Euler equations on the axisymmetric flow surface of varying thickness and radius. The viscous flow zone, consisting of boundary layers and wakes is then modeled using integral boundary layer theory[6]

The assumed operating conditions are those presented in Table 2.1. To summarize, the hub to tip ratio is 0.85, the incoming flow has no swirl component, and the meanline streamline is located between 51% and 58% span as shown in Figure 4-1. Additionally, the flow entering and exiting the blade row is subsonic. The MISES solution constraints used were inlet slope and the leading and trailing-edge Kutta conditions, with corresponding solution variables of inlet and outlet flow slope and leading-edge stagnation location.

Three potential performance metrics were considered as the basis for tolerance op-

[1]Each case, defined as one set of operating conditions, has an execution time of 3-10 seconds on a Pentium 4, 2.4 GHz processor

timization: minimum airfoil loss, loss at nominal flow angle, and incidence range. A metric measuring both airfoil robustness (here defined as robustness to perturbations in inlet flow) and overall performance was desired. Incidence range is traditionally defined as the range of angles over which the total pressure loss is less than twice the minimum[4]. While incidence range is a good measure of robustness to incidence variations, it is not necessarily correlated with minimum loss or loss at nominal flow angle (deterministic measures of performance), and therefore is not a good indicator of overall performance. As such, a hybrid parameter is proposed. This hybrid parameter is defined as the range of incidence angles over which the perturbed airfoil loss is less than twice that of the nominal airfoil's minimum loss. This parameter, referred to as incidence range based on nominal loss, automatically penalizes airfoils whose minimum loss is greater than nominal loss. Figure 4-2 shows the two separate mechanisms that impact incidence range based on nominal loss. Figure 4-2(a) shows the impact of a reduction in traditional incidence range on incidence rage based on nominal loss. The solid line represents loss versus incidence angle for the nominal airfoil. The dotted line represents a perturbed airfoil that has reduced robustness to incidence angle variations. Because both airfoils have the same minimum loss, the incidence range based on nominal loss is equivalent to traditional incidence range for both airfoils. Figure 4-2(b) shows the impact of an increase in minimum loss. The solid line again represents the nominal airfoil. The dotted line in this case represents loss versus incidence angle for an airfoil whose traditional incidence range is the same as the nominal airfoil, but whose minimum loss is greater. The net result is a reduction in incidence range based on nominal loss, thus showing how this hybrid parameter incorporates both changes in robustness.

4.2 Airfoil Tolerancing

This section details the geometric parameters used during optimization and the algorithms used to quantify each parameter.

Table 4.1 summarizes each of the 14 measured parameters used to describe an

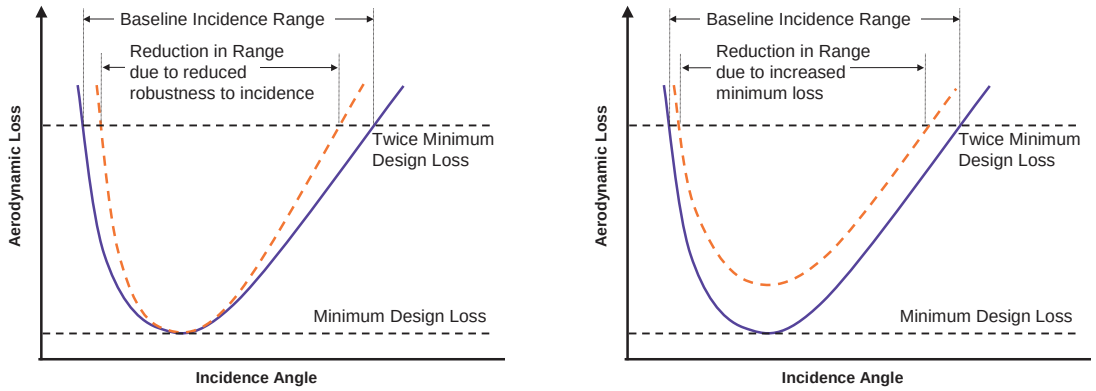

(a) (b)

Figure 4-2: Incidence range based on nominal airfoil loss

airfoil geometry.

While the lengths, angles and thicknesses are familiar to most, the remaining geometric parameters are more abstract. The first step in calculating any of the geometric parameters is to first align the measured airfoil with the nominal airfoil. This involves translating and rotating the measured geometry until the square of the distance between corresponding points is minimized. The rotation is stored as the *Twist* parameter.

The trailing-edge (TE) of each geometry, the last approximately 3% of chord length, has been truncated to facilitate aerodynamic simulations. As such, the chord length is defined as the distance between the leading-edge (LE) point and the truncated trailing edge, the furthest point from the LE, and represents approximately 97% of the full chord length. The chord angle is defined as the angle between the chord, defined above, and the plane of the cascade inlet. The LE angle is defined as the angle the LE makes with the axial inflow direction. The LE and TE thicknesses are defined at 3% and 97% of chord respectively. These five parameters are labeled in Figure 4-3.

The remaining eight parameters measure the curve quality of the measured airfoil relative to the nominal geometry. Two types of curve quality measurements are

Calculated Geometric Parameters		Units
Twist	Relative orientation of measured airfoil	Degrees
Chord Length	Length from LE to TE	Inches
Chord Angle	Angle of chord line relative to plane of inlet	Degrees
LE Angle	Angle of LE relative to axial	Degrees
LE Thickness	Thickness of airfoil at 3% chord	Inches
TE Thickness	Thickness of airfoil at 97% chord	Inches
Max LE Profile	Greatest outward perturbation at LE	Inches
Min LE Profile	Greatest inward perturbation at LE	Inches
Max PS Profile	Greatest outward perturbation on PS	Inches
Min PS Profile	Greatest inward perturbation on PS	Inches
Max SS Profile	Greatest outward perturbation on SS	Inches
Min SS Profile	Greatest inward perturbation on SS	Inches
PS Contour	Measure of curve quality on PS	$Inches^2$
SS Contour	Measure of curve quality on SS	$Inches^2$

Table 4.1: Geometric parameters, definitions and units

calculated: profile measurements and contour measurements. Profile parameters are calculated for each of three airfoil curve sections: the leading-edge (LE), defined by the first 5% of chord; the pressure side (PS), defined as 5%- 97% chord of the airfoil's pressure side; and the suction side (SS), defined as 5%-97% of chord on the airfoil's suction side. Contour measurements are calculated on two airfoil curve sections: the pressure side and suction side.

Profile measurements measure the maximum deviation of the measured airfoil normal to the nominal airfoil surface. Maximum profile measurements measure deviations outward from the nominal surface and minimum profile measurements measure the deviation inward from the nominal surface. Figure 4-4 shows the leading-edge section of an airfoil. On the left, the LE section is shown as the nominal geometry bounded by two parallel curves representing the maximum and minimum observed profile measurements for a measured airfoil. The graphic on the right shows the same LE section overlaid with a measured airfoil. The maximum outward deviation of the airfoil on the LE section corresponds to the maximum LE profile curve and the maximum inward deviation of the measured airfoil on the LE section corresponds to the minimum LE profile curve.

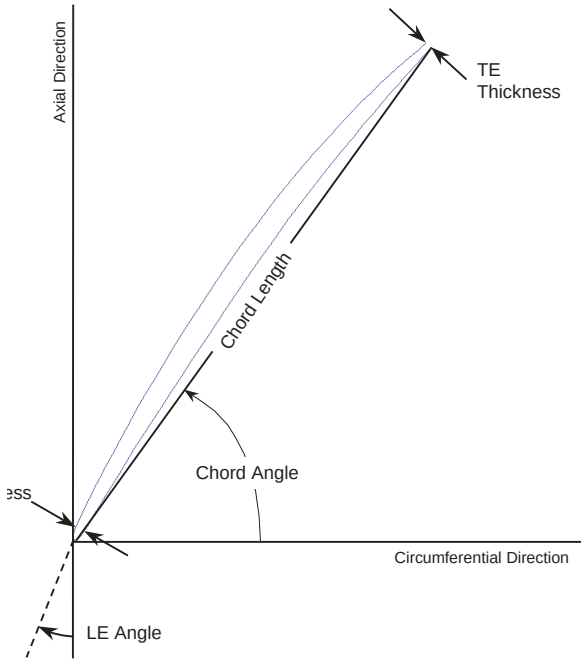

Figure 4-3: Airfoil labeled with common geometric parameters

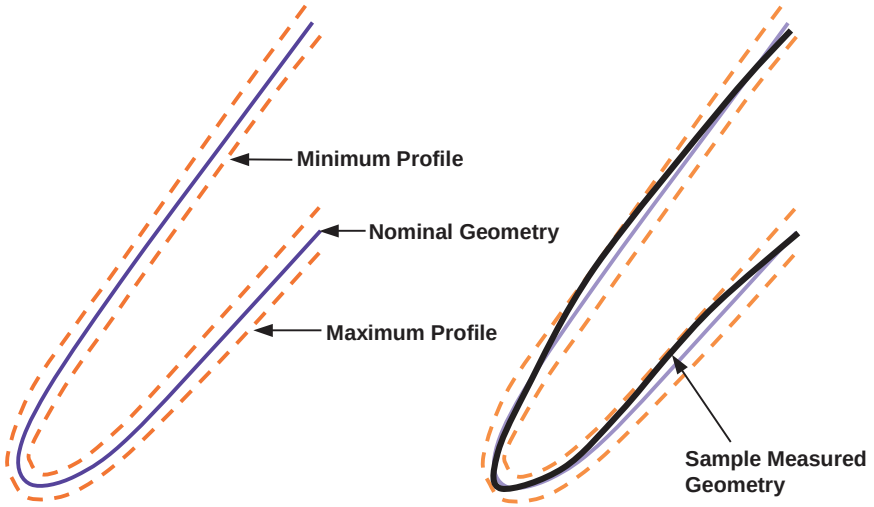

Figure 4-4: LE profile bounds and example measured geometry

For each of the three airfoil sections, a maximum and minimum profile measurement is recorded. The remaining two geometric parameters are the aforementioned contour parameters; one each for the pressure side and suction side. Contour measurements represent the sum of the squares of the distances between corresponding points. Where as the profile measurements indicate the maximum distance, the contour provides information on how well the manufactured blades matches the nominal blade in a root-mean-squared sense.

4.3 Tolerance Optimization

Tolerance optimization takes inputs from the aerodynamic and geometric data for the entire airfoil sample and finds an optimal set of geometric parameter limits based on the chosen performance metric. In this section, both the metric and method of optimization are discussed.

4.3.1 Metric of Optimization

In principle, tolerances are in place to improve the *quality* of manufactured blades. The goal of tolerance optimization then is to select a set of tolerances that maximize the quality of the accepted blades. To choose a metric of optimization is to define the measure of *quality* to be maximized. In principle, the most interesting metric of optimization would quantify the relative costs of accepting a low performing blade and rejecting high performing blades so as to minimize the cost of decisions made during quality control. However, the data required to compute, or even accurately estimate such costs were not available. More achievable metrics might weight airfoils according to their performance and then try to maximize the value of the accepted blades. For example, increasingly larger positive values would be assigned to airfoils exceeding the desired performance limit and increasingly negative values would be assigned to those airfoils below the performance limit with the goal of maximizing the overall value of the selected blades. When the assigned values are linear, this reduces to maximizing the average airfoil performance, however, the assigned values

need not be linear, creating a situation with greater penalties for accepting airfoils with performances well below the desired level.

The metric of optimization ultimately chosen was the probability of incorrect decision. An incorrect decision is defined as one that accepts a low performing airfoil or rejects a high performing airfoil. The probability of incorrect decision was ultimately chosen because it did not require any further information or assumptions and is a objective measure of tolerance effectiveness. Equation 4.1 shows the formula used to calculate the probability of incorrect decision, P,

$$P = \frac{N_A^- + N_R^+}{N_{TOTAL}} \tag{4.1}$$

where N_{TOTAL} is the total number of airfoils inspected, N_A^- is the number of airfoils accepted that do not meet the performance limit, and N_R^+ is the number of airfoils rejected that meet or exceed the performance limit. Note that in Section 3.1 P referred to the actual probability of occurrence and $\hat{P}$ was the probability calculated using a limited sample size. The P in Equation 4.1 is equivalent to $\hat{P}$. This new notation will be used in the remainder of this thesis.

Figure 4-5 is a histogram of incidence range for a given blade sample. The vertical line denotes a desired performance limit about which tolerances are optimized. Those airfoils below the performance limit are denoted as "−" and those above the limit are denoted as "+". Referring back to Equation 4.1, incorrect decisions are defined as accepting "−" blades or rejecting "+" blades.

4.3.2 Method of Optimization

Three different optimization methods were employed during the course of research. These three steps represent the search for a method robust enough to handle the problem and produce a trustworthy answer. The advantages and disadvantages of each method are discussed as they relate to the optimization problem.

The chosen metric of optimization, probability of incorrect decision, is neither linear, nor continuous in terms of the geometric tolerances. During optimization, each

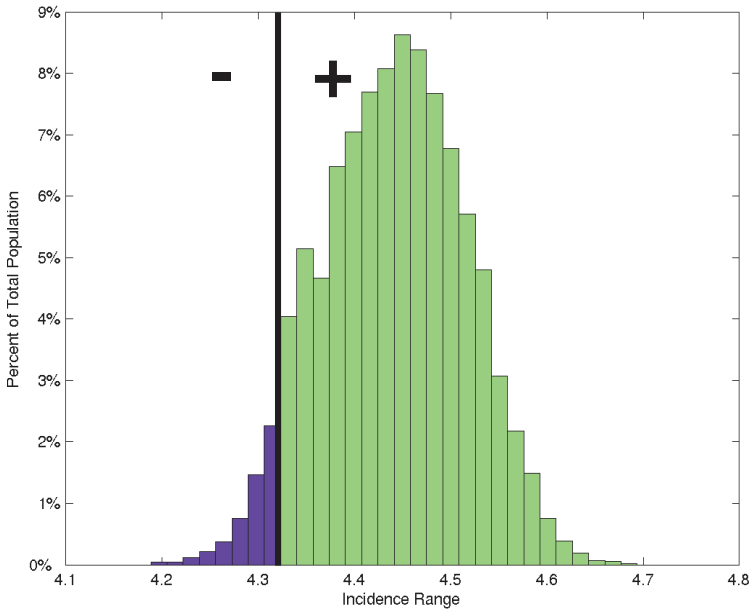

Figure 4-5: Histogram of incidence range with performance limit indicated

airfoil is described by an array consisting of 14 measured parameters and one aerodynamic parameters. Optimization is achieved by placing upper and lower limits on the 14 geometric parameters in order to discriminate between high and low performing airfoils. This results in an optimization problem with 28 degrees of freedom.

Direct Search

One optimization method employed was a nonlinear unconstrained minimization scheme using the Nelder-Mead (direct search) simplex method. The specific algorithm, *fminsearch*, was chosen from the Matlab Optimization Toolbox for its ability to robustly handle non-continuous functions [17]. The simplex method works by first selecting $n+1$ trial points, where n is the number of variables in the problem, here 28. These $n+1$ points enclose a solution space in n-dimensional space. Optimization is then achieved by constantly identifying, and replacing the least desirable vertex, causing the set of $n+1$ points to move closer and closer together, thus converging on a solution point. The downfall to simplex optimization methods is that the solu-

tion space moves in only one direction, and is susceptible to converging on local, as opposed to absolute function minima. Early implementation of *fminsearch* found the local minima problem to be an issue in optimizing tolerance limits. So, despite the methods relatively quick computational time (on the order of one hour for a single solution) use of direct search was discontinued.

"One at a Time" Optimization

"One at a time" optimization was originally employed as a local minima test for results of unconstrained minimization. "One at a time" optimization is executed by varying each parameters one by one in some preset order.

During optimization, the current parameter is varied and the value for which the objective function is minimized replaces the previous parameter value. The process is repeated for each parameter in the order designated. Note, this method differs from independently varying the parameters because the optimized value of a parameter is then used as an input while optimizing the next parameter, thus making the order of optimization important. "One at a time" minimization is in no way guaranteed to give the absolute minima of a function, and was only intended as a means to test the results of direct search optimization. However, the results of "one at a time" minimization continually proved superior to those from direct search, and in an attempt to increase the robustness of "one at a time", it was used in conjunction with direct search minimization. Due to its lack of mathematical rigor, "one at a time" minimization was ultimately discarded in favor of the third and final minimization method applied. The resource requirements for "one at a time" optimization were higher than unconstrained minimization (on the order of several hours for a single solution), and the method employed elements of subjective decision making–such as the order in which to vary parameters and the step size taken during optimization.

Simulated Annealing

The final optimization method used was simulated annealing. Simulated annealing is based on an analogy with the cooling of metals. As metals cool, the atoms rearrange,

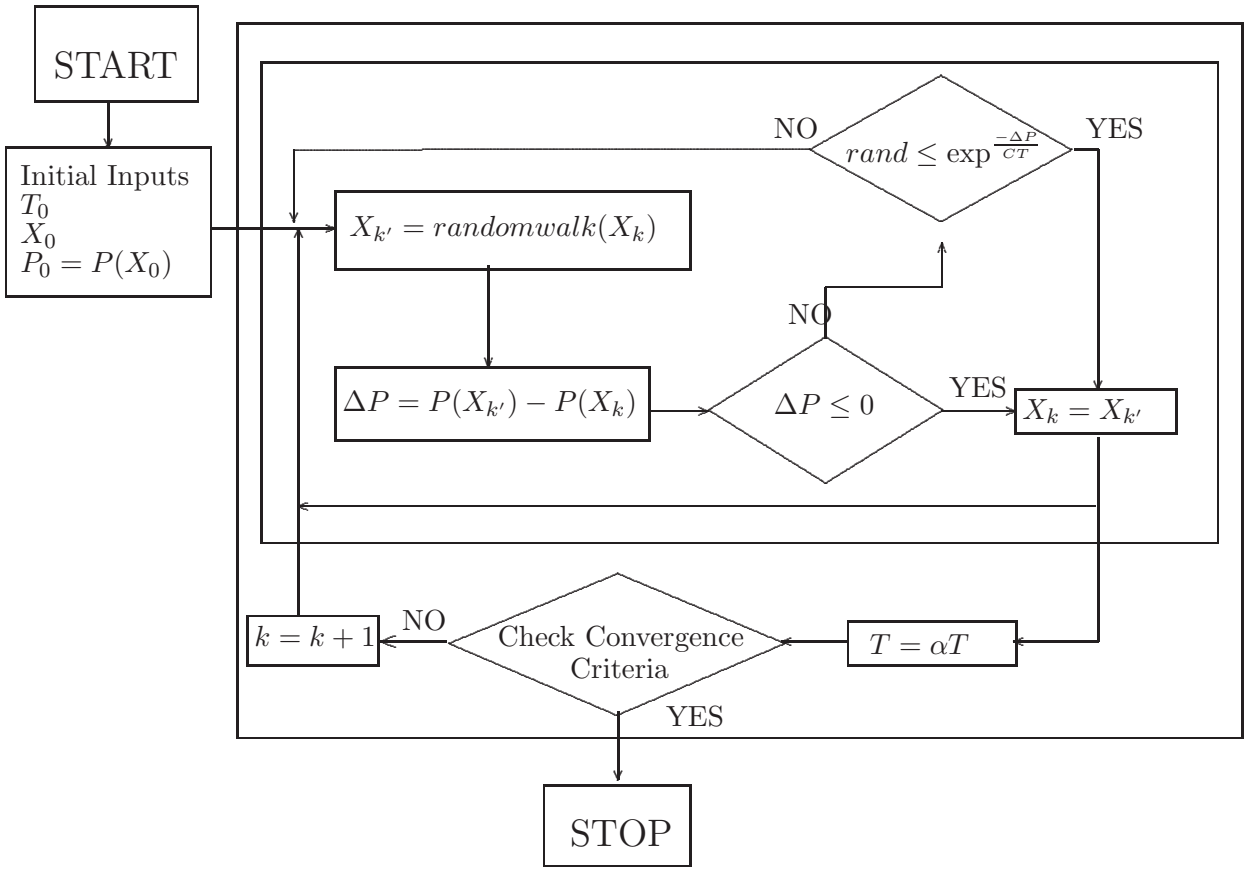

Figure 4-6: Simulated annealing flow chart

seeking a minimum energy configuration. The strength of simulated annealing is that like atoms in a cooling metal, the energy state, or objective function, is allowed to probabilistically rise, thus avoiding the problem of settling into local minima[3]. As the metal temperature cools, jumps in energy level become increasingly unlikely.

Simulated annealing treats increases in the objective function as a rise in energy level. The likelihood, L, of any given energy level, E_r, occurring is dependent on the metal temperature, T, and k_B, Boltzmann's constant,specifically,

$$L(E_R) = \exp^{-\frac{E_R}{k_B T}} . \tag{4.2}$$

As the temperature, T, decreases, the likelihood distribution collapses to some minimum energy state. When simulated annealing is applied to the minimization of

an objective function, some initial temperature and a constant, C, to take the place of k_B are specified. As optimization proceeds, T is gradually reduced to direct the objective function to its minimum value.

The simulated annealing algorithm, shown in Figure 4-6, consists of two nested loops. The outer loop controls the cooling cycle. The inner loop constantly reevaluates the objective function while subjecting the input to random perturbations. If the random perturbation results in a lower function value, the changes are saved and input to the next iteration. If the objective function value increases, the increase in probability, ΔP, and cycle temperature, T, are used to calculate a parameter, L, that is compared to a randomly drawn number between 0 and 1. If the randomly drawn number is less than L, the objective function inputs are saved as inputs to the next iteration. Otherwise, the changes are discarded and the inner loop continues to iterate upon the objective function inputs. Function 4.3 shows the form of Equation 4.2 used in simulated annealing.

$$L = \exp^{-\frac{\Delta P}{CT}} \tag{4.3}$$

Whereas T and k_B have a physical bases in Equation 4.2, the corresponding T and C in Equation 4.3 are quantities chosen to achieve a desired rate of convergence. Based on the magnitude of probabilities under consideration (1%-20%), an initial temperature $T = 273$ and constant $C = 3.86e(-4)$ were chosen. This combination results in an initially ninety-percent chance of allowing a $\Delta P = 1\%$ increase in the probability of incorrect decision.

After some experimentation, a cooling schedule with $\alpha = 0.9$ was chosen. That is, every time the outer loop is called, the temperature returned to the inner loop is 90% of the previous temperature. As the temperature is lowered, Equation 4.3 shows that for a given ΔP, L becomes smaller, thus decreasing the likelihood that an increase in objective function will be allowed.

The traditional convergence criteria is to end optimization when the incremental changes in the objective function become very small. In terms of this optimiza-

tion process, the probabilities being manipulated are themselves small, making the application of this convergence criteria difficult. Instead, simulated annealing was terminated after 2,000 iterations. At this point, the solutions obtained were as good or better than those obtained using direct search or "one at a time" optimization methods.

The benefits of simulated annealing are its robustness to discontinuities combined with the ability to avoid local minima. The greatest disadvantage is the solution time. Most solutions required two or three days to achieve the convergence criteria.

Chapter 5

Results

This chapter discusses the results of tolerance optimization.

5.1 Tolerance Effectiveness

The tolerance optimization results presented in this section were obtained from a probabilistic blade sample based on the original (ORG) blade definition. Tolerances were optimized about seven performance limits chosen so as to designate the $L\%$ of the airfoils with the lowest incidence ranges in the sample as undesirable. The seven chosen limit values, L, were 20%, 15%, 10%, 7.5%, 5%, 2%, and 1%. These values were chosen to represent somewhat realistic part rejection rates within the range of probabilities that could be confidently calculated given error on the Monte Carlo simulations due to limited sample size. Given a probabilistic sample size of 10000 blades, the uncertainty associated with probabilities lower than 1% makes consideration of smaller L values impractical.

Figure 5-1 shows the results of tolerance optimization on the ORG blade sample at each of the seven performance limits defined above. The plain solid line indicates the percent of blades beyond the performance limit, which is L. This is equivalent to the probability of incorrect decision when no tolerances are applied and is used as a benchmark against which to measure tolerance effectiveness.

The dotted-solid line on Figure 5-1 indicates the probability of incorrect decision, P, when optimized tolerances are applied. Differences between L and P are one

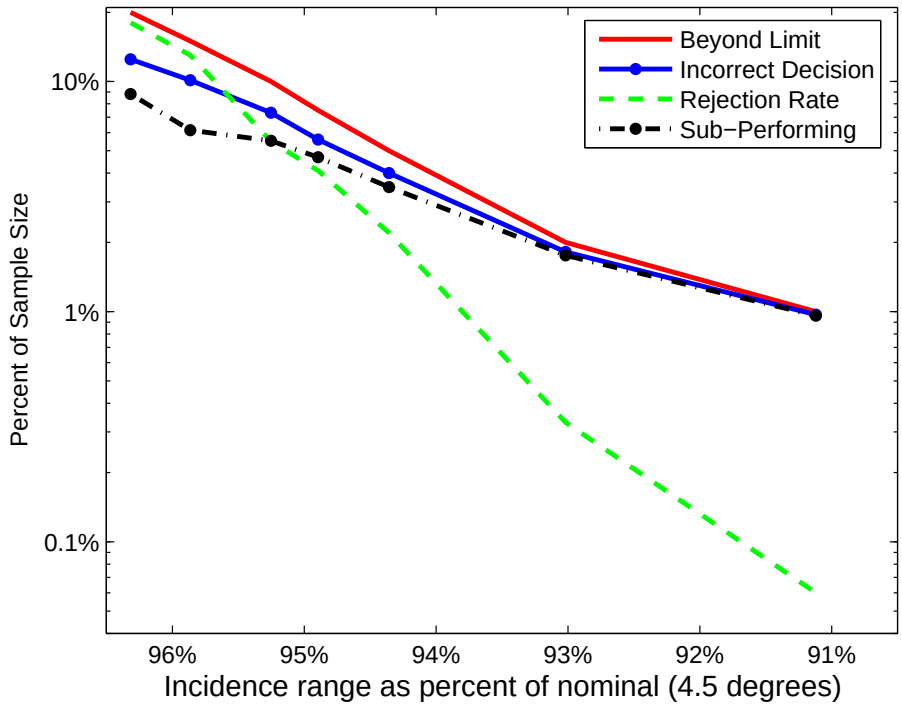

Figure 5-1: Tolerance effectiveness as a function of performance limit for ORG blade sample

measure of how tolerances improve the quality control decision making process.

The plain-dashed line in Figure 5-1 shows the rejection rate obtained when optimized tolerances are applied. The rejection rate is defined as the sum total of desirable and undesirable blades that are rejected, $N_R^+ + N_R^-$, as a percent of the total blade sample size, N_{TOTAL}.

The final line in Figure 5-1, the dotted-dashed line, shows SP, the percent of sub-performing blades among the accepted blades when optimized tolerances are applied,

$$SP = \frac{N_A^-}{N_A}. \tag{5.1}$$

A second measure of tolerance effectiveness is the difference between the initial fraction of sub-performing blades, L, and SP, the fraction after tolerances are applied. Large reductions in SP relative to L indicate the accepted blades have a higher quality, $(Q = \frac{N_A^+}{N_A})$, than the original sample.

The ORG sample shows improvements in sample quality when tolerances are applied at high performance limits, for example at 96.5% of nominal incidence range, $SP = 9\%$, less than half the 20% value obtained when no tolerances are applied. This corresponds to an improvement in sample quality of 11%. The improvement in sample quality, however, comes at the cost of a 19% rejection rate. When the performance limit is at 94% of nominal incidence range and lower, the improvements in sample quality and the decision making process are statistically insignificant.

The main point of Figure 5-1 is that tolerances are more effective at aggressive performance limits (ex: 96.5% nominal incidence range), than at lower, less aggressive performance limits (ex: 93% nominal incidence range). Said another way, there is a significant improvement in accepted sample quality at $L >= 5\%$. Improvements in sample quality quickly approach zero at smaller L values, the L regime this blade was presumably designed for. As such, the current practice of thoroughly inspecting all blades that fail quality control is a necessary precaution to protect against the limits of tolerance effectiveness.

Table 5.1 shows how the rejection decisions were spread among the different geometric parameters used in tolerancing. While a blade need violate only one parameter limit to be rejected, a rejected blade may violate several parameter limits. In the table, parameter strength is defined as the number of blades violating a given parameter as a percent of the total number of rejected blades.

Strength of Geometric Best Discriminators				
L	LE thickness	Maximum LE profile	Pressure contour	Suction contour
20	73%	4%	13%	53%
15	48%	2%	13%	44%
10	55%	4%	10%	33%

Table 5.1: Strength of geometric best discriminators for ORG blade sample

The top four parameters accountable for blade rejections are leading-edge (LE) thickness, maximum LE profile, and both the pressure and suction side contour measurements. Of interest is that the parameter strengths vary with performance limit. The relative order of strengths does not change, but as the performance limit is

lowered, the decisions making appears to be spread more evenly among parameters, indicating that no one parameter can be too heavily relied upon for making quality control decisions. Table 5.2 shows the decision quality of each parameter. Parameter quality describes the percent of rejection decisions that resulted in the rejection of a poor-performing blade. The decision quality appears relatively independent of performance limit.

Quality of Geometric Best Discriminators				
L	LE thickness	Maximum LE profile	Pressure contour	Suction contour
20	75%	84%	80%	80%
15	78%	88%	72%	72%
10	77%	83%	85%	84%

Table 5.2: Quality of geometric best discriminators for ORG blade sample

5.2 Impact of Probabilistic Design on Tolerancing

The impact of probabilistic robust design on tolerance effectiveness is presented in this section. The results shown are based on the deterministic minimized loss (DML) and the minimized standard deviation of loss (MSL) blade redesigns. The ORG blade cannot be used in direct comparison because its actual design methods and objectives are unknown.

Figures 5-2 and 5-3 provide separate treatments of the optimization results from each blade sample using the same format as Figure 5-1.

Figure 5-2 shows an overall decrease in tolerance effectiveness for the DML blade sample as compared to the ORG blade sample. The implication is that tolerance effectiveness is design dependent. Even at the 95.5% nominal incidence range performance limit, the improvement in sample quality when optimized tolerances are applied is only a 6% reduction in the poor-performing blades. Improvements in sample quality attributed to tolerances are insignificant by 94% of nominal incidence range.

For the robust blade, Figure 5-3 shows tolerance effectiveness levels comparable to those for the DML blade sample. This implies that probabilistic robust design does

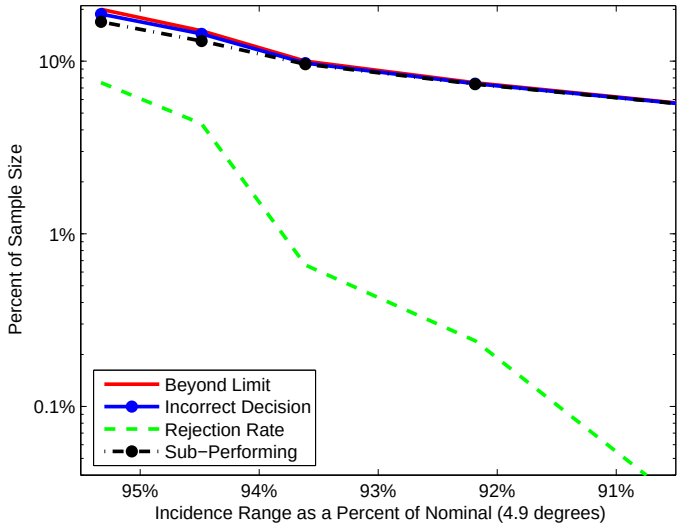

Figure 5-2: Tolerance effectiveness as a function of performance limit: Deterministic redesign

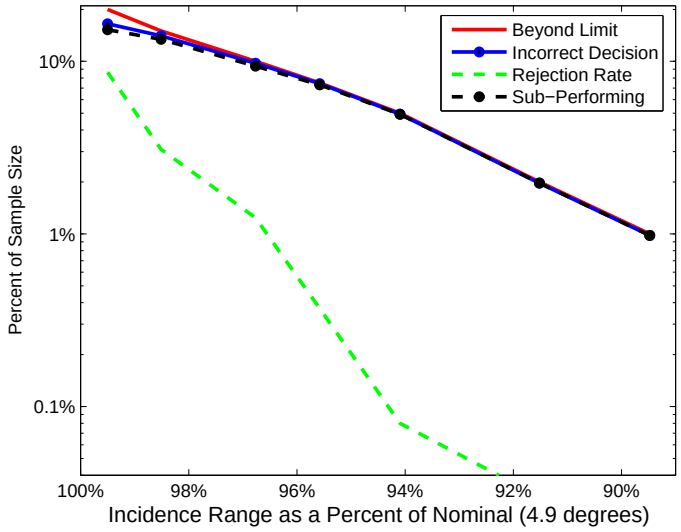

Figure 5-3: Tolerance effectiveness as a function of performance limit: Probabilistic redesign

not adversely effect tolerance effectiveness. The maximum improvement in sample quality is 8% and occurs at the 99% performance limit; the limit at which $L = 20\%$. This is in contrast to the DML blade sample, where $L = 20\%$ corresponds to a performance limit at 95.5% of nominal incidence range and the improvement in overall sample quality is 6%.

Table 5.3 shows a comparison of best discriminators for $L = 10\%$. The same top four geometric parameters that best predicted performance for the ORG blade sample are again important in both the DML and MSL blade samples. At more aggressive performance limits, chord length becomes a stronger parameter than LE thickness in the DML sample. Maximum LE profile is the best discriminator for the deterministic blade with pressure contour coming in a distant second. However, the probabilistically redesigned blade has a more even strength distribution between three geometric parameters: maximum LE profile, pressure side contour, and suction side contour. This emphasizes that those geometric parameters that best predict aerodynamic performance are design dependent. This means that no one parameter should ever become a quality control favorite because even small changes in design could render that parameter less effective. Rather, a group of several trusted parameters is required for effective tolerancing.

Strength of Geometric Best Discriminators				
Design	LE thickness	Maximum LE profile	Pressure contour	Suction contour
DML	8%	72%	28%	2%
MSL	1%	27%	52%	50%

Table 5.3: Strength of geometric best discriminators for DML and MSL blade samples at $L = 10\%$

Figures 5-4 and 5-5 present a direct comparison of the tolerance effectiveness for the deterministically and probabilistically designed blades. Figure 5-4 shows a comparison of rejection rates and incorrect decision probabilities as functions of performance limit expressed as a percent of nominal incidence range. The MSL blades show incorrect decision probabilities that are half of the deterministic blades for a given performance limit and rejection rates that are an order of magnitude smaller

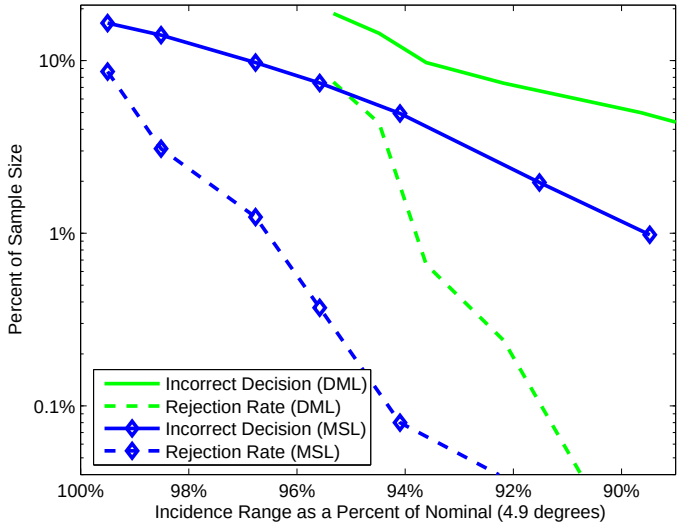

Figure 5-4: Impact of probabilistic design on tolerance effectiveness: Performance limit expressed as percent of nominal incidence range

than their DML counterparts. However, as Figure 5-5 shows, these improvements are in fact due to a reduction in the standard deviation of incidence range in the MSL blades due to robust design. In Figure 5-5, the probability of incorrect decision and rejection rates are plotted as functions of performance limit expressed as the number of standard deviations from the nominal incidence range.

5.3 Impact of Process Precision on Tolerancing

This section investigates the impact of manufacturing precision on tolerance effectiveness. The results are based on the ORG blade with the nominal manufacturing variability level and twice the nominal manufacturing variability level. Amplification of the variability level was achieved by doubling the modal amplitudes calculated using the methods outlines in Section 3.2.

Figure 5-6 shows the metrics of tolerance effectiveness as a function of performance limit for blades based on the original blade profile subjected to twice the observed manufacturing variability (ORG_2). The plot is organized in the same manner as Figure 5-1. The improvement in sample quality when tolerances are applied is 10% at

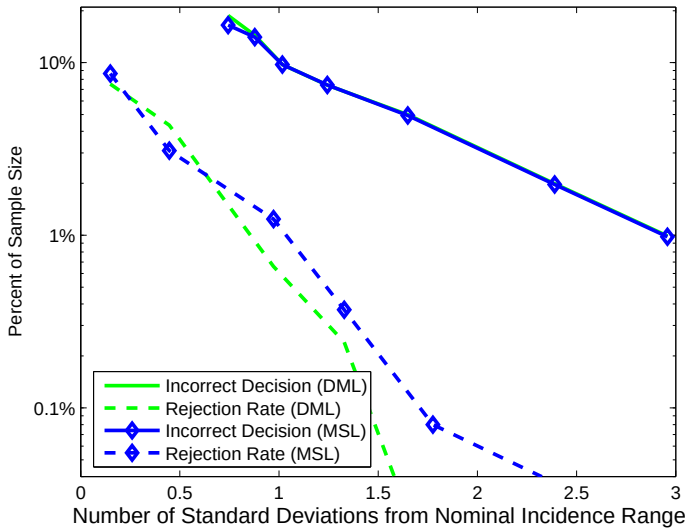

Figure 5-5: Impact of probabilistic design on tolerance effectiveness: Performance limit expressed in standard deviations from nominal incidence range

the 94% nominal incidence range performance limit and slowly reduces to 0.1% at the 85% performance limit. While the effectiveness of applying tolerances does decrease with less aggressive performance limits, tolerances applied at the less aggressive performance limits show greater improvements in sample quality in the ORG_2 sample than in the ORG sample.

Table 5.4 shows the change in best discriminator when the manufacturing variability is doubled. In both cases, the most important parameter is LE thickness. However, the second most important parameters, which are not far behind in strength, change with increased variability. At the nominal variability level, suction side contour is an important indicator of aerodynamic performance. When the variability is doubled, the second best indicator of performance becomes maximum LE profile. Therefore, the best geometric discriminators of performance are also dependent on manufacturing precision.

Figures 5-7 and 5-8 directly compare tolerance effectiveness for blade samples with one and two times nominal manufacturing variability. Figure 5-7 shows the probability of incorrect decision, P, when optimized tolerances are applied and the resulting rejection rates as a function of performance limit expressed as a percent of

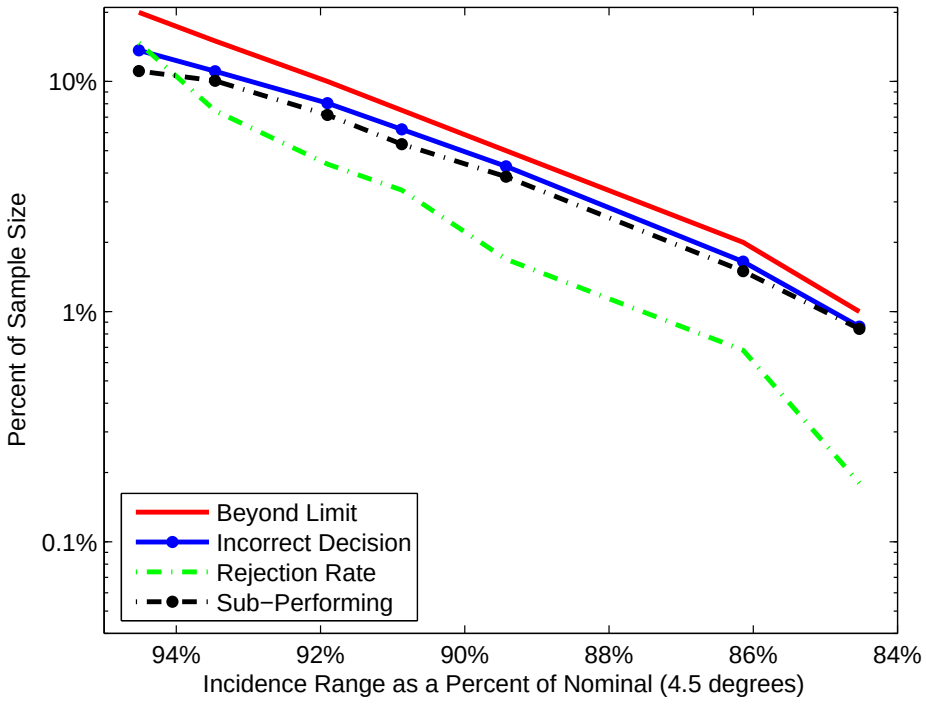

Figure 5-6: Tolerance effectiveness as a function of performance limit: Original blade design with twice nominal manufacturing variability

Strength of Geometric Best Discriminators				
Design	LE thickness	Maximum LE profile	Pressure contour	Suction contour
ORG_1	55%	4%	10%	33%
ORG_2	64%	46%	6%	3%

Table 5.4: Strength of geometric best discriminators for original and increased variability blade samples at $L = 10$

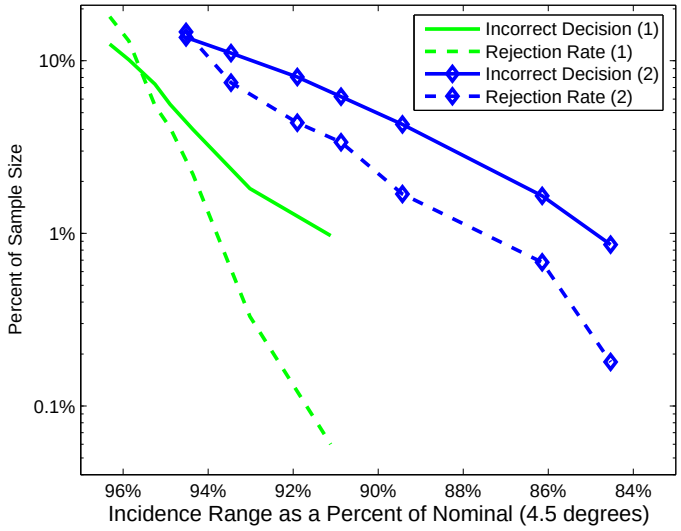

Figure 5-7: Impact of process precision on tolerance effectiveness: performance limit expressed as a percent of nominal incidence range

nominal incidence range. As expected, the blade sample with lower variability has probabilities, P, that are on the order of one-third to one-tenth that of the greater-variability blade sample. In addition, the rejection rates are an order of magnitude lower. However, as Figure 5-8 shows, when the performance limits are expressed as a function of standard deviations from nominal performance, the measures of tolerance effectiveness overlap. The implication is that, for the example shown, changes in manufacturing precision do not impact tolerance effectiveness.

5.4 Probabilistic Design versus Process Precision

This, the last section in Chapter 5, shows the impact of robust design in contrast to improving process precision. The blade samples used for this comparison are based on

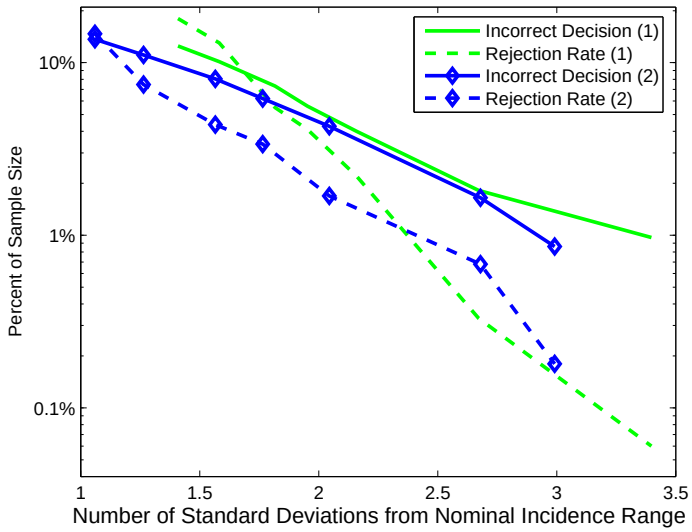

Figure 5-8: Impact of process precision on tolerance effectiveness: performance limit expressed in standard deviations from nominal incidence range

a deterministic blade with nominal manufacturing levels (DML_1), and a probabilistic redesign blade with twice the nominal manufacturing variability (MSL_2).

As shown in Figure 5-9, the performance distributions for probabilistic samples based on the DML_1 and MSL_2 blades are similar. The DML_1 sample incidence range distribution (Figure 5-9(a)) has an 8% higher standard deviation than the MSL_2 sample. In addition to the similarities in aerodynamic performance, the optimized tolerances also behave similarly for both samples. Figure 5-10 shows the P obtained when optimized tolerances are applied and the corresponding rejection rates for both blade samples. The differences between the lines are minimal, implying that from a quality control standpoint implementing robust design on this blade is equivalent to halving the manufacturing variability. That both the performance distribution and tolerancing effectiveness are similar is important because reducing manufacturing variability can be expensive, be it necessary to purchase or use more expensive high-precision machinery or to make additional tool passes to improve surface finish. Robust design offers a way to improve part quality given fixed manufacturing capabilities, and does so without adversely affecting current quality control procedures.

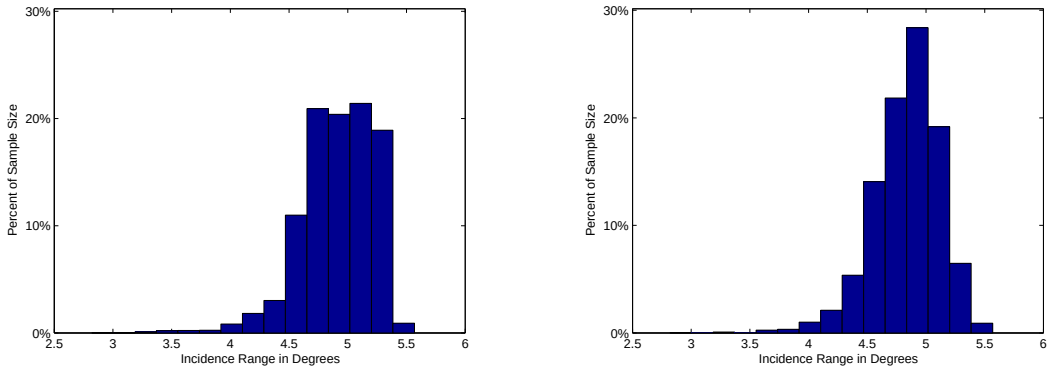

(a) Incidence range distribution of DML_1 probabilistic sample

(b) Incidence range distribution of MSL_2 probabilistic sample

Figure 5-9: Comparison of incidence range distribution for DML_1 and MSL_2 samples

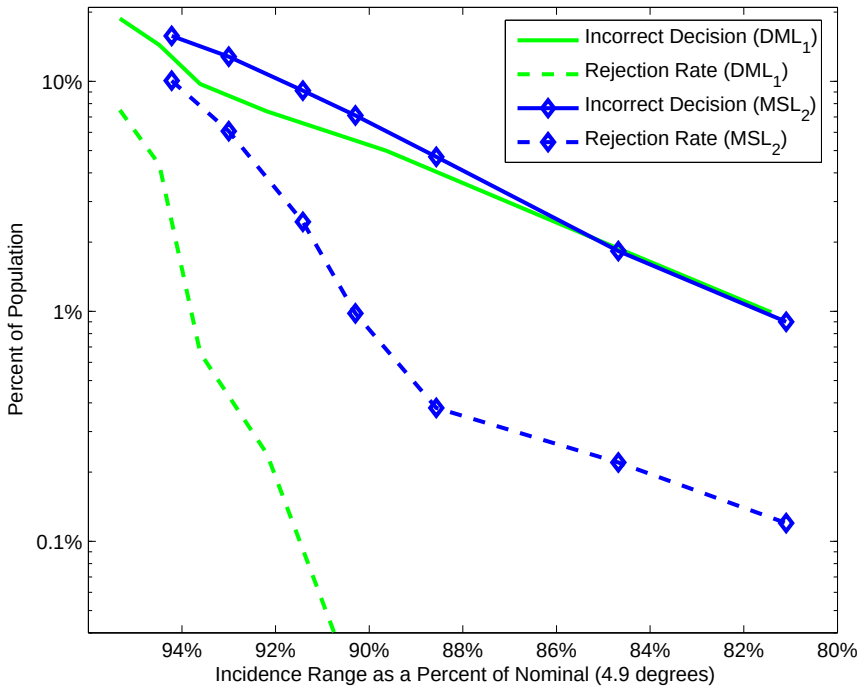

Figure 5-10: Tradeoff in tolerance effectiveness between increased manufacturing variability and probabilistic design

Chapter 6

Conclusions and Suggestions for Further Investigation

In this chapter are presented a brief discussion of the limitations of this research, the conclusions, and a few suggestions for future research.

6.1 Limitations of Work

The primary limitation of this work is that only one set of manufacturing data were used to generate high-speed results. While a second set of manufacturing data was available, the fan blades, the operating conditions created a much less robust solution process, especially when including geometric variability. The inclusion of an additional, geometrically mode-dominated blade set would allow for additional investigation into the impact of probabilistic design and variability levels.

The second limitation pertains to analyzing only the meanline streamline. Referring back to Figure 3.2.2, the mean perturbation of the compressor blade is larger at the blade tip in comparison to the mean line streamline. The same pattern is observed in the fan data, where the manufacturing variability is greatest between 70% span and the blade tip.

Where as the two previous limitations pertain to interpretation of results, the next limitation pertains to application. In this research, the tolerances were all optimized based on actual airfoil performance. This required a priori knowledge of manufactur-

ing perturbations and the time and resources to run thousands of test airfoils through aerodynamic analysis. In a real manufacturing situation, similar advanced knowledge and computational resources might not be available.

6.2 Conclusions

Despite the limitations presented by data availability, several conclusions can still be drawn.

First, pertaining to tolerance effectiveness, tolerance effectiveness is dependent both on design and performance limit. At aggressive performance limits, tolerances are able to improve upon the quality of the accepted blades, halving the percentage of poor-performing blades in the case of the ORG sample. However, at less aggressive limits, tolerances are of little impact, with optimized rejection rates quickly falling near zero. This suggests that at lower performance limits, the strength of tolerances is in monitoring the health of a manufacturing process as opposed to a means to improve the quality of the accepted blades. The ineffectiveness of tolerances at less aggressive performance limits also solidifies the need for additional procedures to "double-check" blades that fail quality control. While detailed additional analysis is expensive, at less aggressive performance limits, high-performing blades account for a disproportionate number of the blades being rejected.

The second conclusion is that the best discriminators of performance are dependent on design, level of variability, and performance limit. This implies that the key, or most trusted, parameter used during quality control changes with changes in design and manufacturing procedure. As stated in Section 4.2, current quality control practices favor profile measurements above other geometric parameters. While profile measurements faired well, contour parameters and LE thickness were also important parameters. Because the best discriminators change with design and, in several cases, multiple parameters were of approximately equal importance, this research recommends no one parameter be chosen as the single most trusted parameter. Rather, a group of trusted parameters is required to assure tolerances perform at optimal

levels. The suggested parameters are LE thickness, maximum LE profile, and both the pressure and suction side contour measurements.

In a comparison of deterministically and probabilistically designed airfoils, the probabilistically designed airfoil displayed an order of magnitude lower rejection rates for a given incidence range performance limit. However, further investigation shows the benefits of probabilistic design are due wholly to the reduction in standard deviation of the performance distribution. It is interesting to note that the overall effectiveness of the tolerances do not seem to be affected by probabilistic design or changes in the level of manufacturing variability.

On a final note, for the blade considered in this research, the probabilistic design behaves, from both performance and a quality control perspectives, the same as a deterministically designed blade with *half* the manufacturing variability. This indicates probabilistic robust design may have uses as an alternative to increasing manufacturing precision.

6.3 Suggestions for Future Research

Suggestions for future work primarily address the limitations of this work.

1. Address limitations imposed by only evaluating the meanline streamline.
   (a) Analyze several streamlines in areas of interest.
   (b) Perform full 3-D analysis on blades.
2. Evaluate additional blade geometries.
   (a) Include mode-dominated geometries.
   (b) Investigate geometries with greater levels of observed manufacturing variability.
   (c) Analyze similar geometries manufactured using different processes to investigate how choice of manufacturing process affects observed variability.
   (d) Analyze different geometries manufactured using the same process to investigate impact of blade geometry on observed variability.
3. Explore ways to apply robust design and tolerance optimization in situations where a priori knowledge of manufacturing variability is not readily available.

(a) Can observed variability from previous designs be applied to new designs?

(b) Can information obtained during initial production be used to iterate upon both design and optimized tolerance ranges?

Bibliography

[1] R. H. Aungier. *Axial Flow Compressors*. ASME Press, New York, NY, 2003.

[2] C. M. Bishop. *Neural Networks for Pattern Recognition*, chapter 5. Oxford University Press, Oxford, UK, 1995.

[3] B. J. Buckham and C. Lambert. Simulated annealing applications. Retrieved August 2004 from World Wide Web: http://www.me.uvic.ca/žđong/courses/mech620/SA_App.pdf, November 1999.

[4] N. A. Cumpsty. *Compressor Aerodynamics*. Longman, London, UK, 1989.

[5] M. Drela. *Pros and cons of airfoil optimization*, chapter 19, pages 363–380. Fronties of Computational Fluid Dynamics 1998. World Scientific Publishing, 1999.

[6] M. Drela and H. Youngren. *A User's Guide to MISES 2.53*. MIT Fluids Dynamics Research Laboratory, 70 Vassar St. Cambridge, MA 02139, December 1998.

[7] X. Du and W. Chen. Methodology for managing the effect of uncertainty in simulation-based design. *AIAA Journal*, 38(8):1471–8, August 2000.

[8] V. E. Garzon. *Probabilistic Aerothermal Design of Compressor Airfoils*. PhD thesis, Massachusetts Institute of Technology, February 2003.

[9] V. E. Garzon and D. L. Darmofal. Impact of geometric variability on axial compressor performance. *Journal of Turbomachinery*, 125(4):692–703, October 2003.

[10] V. E. Garzon and D. L. Darmofal. On the aerodynamic design of compressor blades for robustness under geometric uncertainty. In *Proceedings of the ASME Gas Turbo Expo*, number GT2004-53581. American Society of Mechanical Engineers, 2004.

[11] J. L. Häcker. Statistical analysis of manufacturing deviations and classification methods for probabilistic aerothermal design of turbine blades. Master's thesis, Diplomarbeit, Department of Aeronautics and Astronautics, University of Stuttgart, Stuttgart, Germany, August 2000.

[12] K. Y. Sanliturk M. Imregun and D. J. Ewins. A probabilistic analysis of single-degree-of-freedom blade vibration. In *Proceeding of ASME Gas Turbo Expo*, number 93-FT-264. American Society of Mechanical Engineers, 2003.

[13] P. J. Drake Jr., editor. *Dimensioning and Tolerancing Handbook*. McGraw-Hill, New York, NY, 1999.

[14] J. L. Kerrebrock. *Aircraft Engines and Gas Turbines*. MIT Press, Cambridge, MA, 1992.

[15] J. Lancaster. Personal Communication, October 2003.

[16] L. Huyse S. L. Padula R. M. Lewis and W. Li. Probabilistic approach to free-form airfoil shape optimization under uncertainty. *AIAA Journal*, 40(9), September 2002.

[17] The Mathworks, Inc, Natick, MA. *Optimization Toolbox User's Guide*, v2.0 edition, 2002.

[18] A. Papoulis. *Probability, Random Variables, and Stochastic Processes*. McGraw Hill, Inc, third edition edition, 1991.

[19] R. W. Preisendorfer. *Principal Component Analysis in Meteorology and Oceanography*. Elsevier, Amsterdam, 1988.

[20] W. B. Roberts. Axial compressor performance restoration by blade profile control. Number 84-GT-232. ASME, 1984.

[21] C. Y. Wu. Arbitrary surface flank milling of fan, compressor, and impellor blades. *ASME Journal of Engineering for Gas Turbines and Power*, (117):534–539, July 1995.

[22] P. N. Koch B. Wujeck and O. Golovidov. A multi-stage parallel implementation of probabilistic design optimization in an mdl framework. In *Proceeding of 8th AIAA/USA/NASA/ISSMO Symposium on Multidisciplinary Analysis and Optimization*, number AIAA-2000-4805, Long Beach, CA, 2000. American Institute of Aeronautics and Astronautics.